Supporting Information

Electron Deficient Dihydroindaceno-Dithiophene Regioisomers for n-Type Organic Field-Effect Transistors

Jean-David Peltier,[a] Benoît Heinrich,[c] Bertrand Donnio,[c] Joëlle Rault-Berthelot,[a*] Emmanuel Jacques[b*] Cyril Poriel[a*]

[a] UMR CNRS 6226-Institut des Sciences Chimiques de Rennes- Équipe Matière Condensée et Systèmes Électroactifs, Bat 10C, Campus de Beaulieu - 35042 Rennes cedex France

[b] UMR CNRS 6164-Institut d'Électronique et des Télécommunications de Rennes- Département Microélectronique & Microcapteurs, Bât.11B, Université Rennes 1, Campus de Beaulieu 35042 Rennes Cedex, France

[c] Institut de Physique et Chimie des Matériaux de Strasbourg (IPCMS), UMR 7504, CNRS-Université de Strasbourg, 23 rue du Loess, BP 43, 67034 Strasbourg Cedex 2, France

joelle.rault-berthelot@univ-rennes1.fr, emmanuel.jacques@univ-rennes1.fr, cyril.poriel@univ-rennes1.fr

Table of content

MOLECULAR STRUCTURE AND NAME OF DIFFERENT COMPOUNDS CITED IN THE TEXT

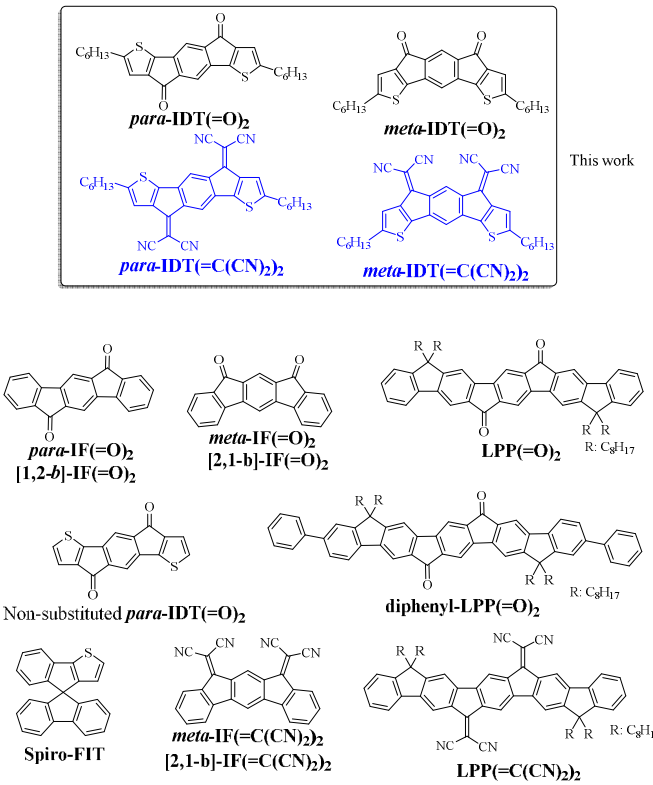

Chart S1: Molecular structure, name or acronym of the different compounds cited in the publication

MATERIAL AND METHODS

Synthesis:

All manipulations of oxygen- and moisture-sensitive materials were conducted with a standard Schlenk technique. Commercially available reagents and solvents were used without further purification other than those detailed below. THF was distilled from sodium/benzophenone prior to use. Light petroleum refers to the fraction with boiling point 40-60°C. 2.5M solution of n-BuLi in hexane was purchased from Sigma Aldrich. 5-hexyl-2-tributylstannylthiophene, Diethyl 2,5-bis[2'-(5'-dihexylthienyl)]-1,4-benzendicarboxylate, 2,5-Bis[2'-(5'-dihexylthienyl)]-1,4-benzendicarboxylic acid, 2,5-Bis[2'-(5'-dihexylthienyl)]-1,4-benzendicarboxylic acid dichloride and 2,7-Dihexyl-4,9-dihydro-s-indaceno[1,2-*b*:5,6-b']dithiophene-4,9-dione were synthesized according to published procedures with spectroscopic analyses and purity in perfect accordance with the literature.[1] Reactions were stirred magnetically, unless otherwise indicated. Analytical thin layer chromatography was carried out using aluminum backed plates coated with Merck Kieselgel 60 GF254 and visualized under UV light (at 254 and 360 nm). Chromatography was carried out using Teledyne Isco CombiFlash® Rf 400 (UV detection 200-360nm), over standard silica cartridges (Redisep® Isco, or Puriflash® columns Interchim). ^{1}H and ^{13}C NMR spectra were recorded using Bruker 300 MHz instruments (^{1}H frequency, corresponding ^{13}C frequency: 75 MHz); chemical shifts were recorded in ppm and J values in Hz. In the ^{13}C NMR spectra, signals corresponding to C, CH, CH_2 or CH_3 groups, assigned from DEPT, are noted, all others are C. The residual signals for the NMR solvents are: $CDCl_3$; 7.26 ppm for the proton and 77.00 ppm for the carbon, CD_2Cl_2; 5.32 ppm for the proton and 53.80 ppm for the carbon, DMSO-D6; 2.45 ppm for the proton and 40.42 ppm for the carbon, Tetrachloroethane-D2; 6.00 ppm for the proton and 73.78 ppm for the carbon. The following abbreviations have been used for the NMR assignment: s for singlet, d for doublet, t for triplet and m for multiplet. High resolution mass spectra were recorded at the Centre Régional de Mesures Physiques de l'Ouest (CRMPO-Rennes) on (i) Waters Q-Tof II or on (ii) Q-Exactive or on (iii) Maxis 4G.

Electrochemical studies:

All electrochemical experiments were performed under an argon atmosphere, using a Pt disk electrode (diameter 1 mm), the counter electrode was a vitreous carbon rod and the reference electrode was a silver wire in a 0.1 M $AgNO_3$ solution in CH_3CN. Ferrocene was added to the electrolytic solution at the end of a series of experiments. The ferrocene/ferrocenium (Fc/Fc^+) couple served as internal standard. The three electrode cell was connected to a PAR Model 273 potentiostat/galvanostat (PAR, EG&G, USA) monitored with the ECHEM Software. Activated Al_2O_3 was added in the electrolytic solution to remove excess moisture. For a further comparison of the electrochemical and optical properties, all potentials are referred to the SCE electrode that was calibrated at 0.405 V *vs*. Fc/Fc^+ system. Following the work of Jenekhe, we estimated the electron affinity (EA) or lowest unoccupied molecular orbital (LUMO) and the ionization potential (IP) or highest occupied molecular orbital (HOMO) from the redox data.[2] Indeed, the LUMO level was calculated as: LUMO (eV)= $-[E_{onset}^{red}$ (*vs* SCE) + 4.4] and the HOMO level as: HOMO (eV) = $-[E_{onset}^{ox}$ (*vs* SCE) + 4.4], based on an SCE energy level of 4.4 eV relative to the vacuum. The electrochemical gap was calculated from: ΔE^{el} =|HOMO-LUMO| (in eV).

Molecular modeling :

Full geometry optimization with Density functional theory (DFT)[3-4] and Time-Dependent Density Functional Theory (TD-DFT) calculations were performed with the hybrid Becke-3 parameter exchange[5-7] functional and the Lee-Yang-Parr non-local correlation functional[8] (B3LYP) implemented in the Gaussian 09 (Revision B.01) program suite[9] using the default convergence criterion implemented in the program. The figures were generated with GaussView 5.0. DFT and TD-DFT calculations at the

B3LYP/6-311+g(d,p) in their respective optimized singlet state (optimization at the B3LYP/6-311+g(d,p) level of theory, infrared spectra were calculated on the final geometry to ascertain that a minimum was obtained *i.e.* no negative frequency). Calculations were carried out at the Centre Informatique National de l'Enseignement Supérieur (CINES) in Montpellier under project c2016085032.

Spectroscopic studies:

Cyclohexane (AnalaR NORMAPUR, VWR) and THF (AnalaR NORMAPUR, VWR) were used without further purification. UV-visible spectra were recorded using a UV-Visible spectrophotometer SHIMADZU UV-1605. The optical gap was calculated from the absorption edge of the UV-vis absorption spectrum using the formula ΔE^{opt} (eV) = hc/λ, λ being the absorption edge (in meter). With h = 6.62606×10^{-34} J.s (1eV = 1.60217×10^{-19} J) and c = 2.99792×10^{8} m.s^{-1}, this equation may be simplified as: ΔE^{opt} (eV) = 1239.84/ λ (in nm).

Thermal analysis:

Thermal Gravimetric Analysis (TGA) was carried out at 10°C/min from 0 to 600°C under nitrogen atmosphere. Differential scanning calorimetry (DSC) was carried out by using NETZSCH DSC 200 F3 instrument equipped with an intracooler. DSC traces were measured at 10 °C/min, 2 heating/cooling cycles were successively carried out. Alternatively, the TGA measurements were carried out with a Q50 apparatus of TA Instruments, at a scanning rate of 5 C min^{-1} and with air as purge gas. The transition temperatures and enthalpies were measured by differential scanning calorimetry (DSC) with a TA Instruments DSC-Q1000 instrument operated at a scanning rates of 1 to 5°C min^{-1} on heating and on cooling.

Self-organization properties:

The SWAXS patterns were recorded with a linear monochromatic Cu Kα1 beam (λ = 1.5405 Å) obtained using a sealed-tube generator (600 W) equipped with a bent quartz monochromator. Patterns were recorded with a curved Inel CPS 120 counter gas-filled detector linked to a data acquisition computer; periodicities up to 70 Å can be measured, and the sample temperature controlled to within ±0.01 °C from 20 to 200 °C. The crude powder was filled in Lindemann capillaries of 1 mm diameter and 10 µm wall thickness and exposure times were varied from 1 to 24 h. The optical textures of the mesophases were studied with a Leitz polarizing microscope (POM) equipped with a Mettler FP82 hot-stage and an FP80 central processor.

SYNTHESIS

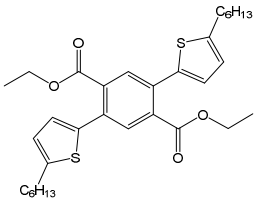

diethyl 2,5-bis(5-hexylthiophen-2-yl)benzene-1,4-dicarboxylate

M.p. N/A, ^{1}H NMR (300 MHz, CD_2Cl_2) δ 7.71 (s, 2H), 6.90 (d, *J* = 3.5 Hz, 2H), 6.76 (dd, *J* = 3.5, 1.0 Hz, 2H), 4.23 (q, *J* = 7.1 Hz, 4H), 2.94 – 2.68 (m, 4H), 1.70 (t, *J* = 7.5 Hz, 4H), 1.48 – 1.25 (m, 12H), 1.19 (t, *J* = 7.1 Hz, 6H), 0.90 (td, *J* = 6.0, 5.2, 2.1 Hz, 6H); ^{13}C NMR (75 MHz, CD_2Cl_2) δ 167.85, 147.66, 137.65, 133.76, 132.91, 131.13 (CH), 126.61 (CH), 124.57 (CH), 61.60 (CH_2), 31.74 (CH_2), 31.58 (CH_2), 30.08 (CH_2), 28.79 (CH_2), 22.61 (CH_2), 13.70 (CH_3), 13.65 (CH_3). IR (ATR, cm^{-1}): v=457, 530, 536, 619, 669, 692, 721, 804, 841, 899, 927, 999, 1045, 1105, 1169, 1234, 1255, 1278, 1379, 1463, 1558, 1580, 1718, 2340, 2361, 2580, 2617, 2660, 2723, 2854, 2924, 2953, 3196

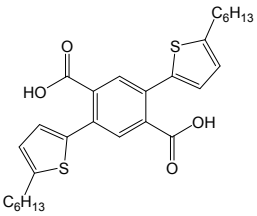

2,5-bis(5-hexylthiophen-2-yl)benzene-1,4-dicarboxylic acid

M.P.155-156°C, ^{1}H NMR (300 MHz, DMSO-d_6) δ 13.34 (s, 2H), 7.61 (s, 2H), 7.05 (d, *J* = 3.6 Hz, 2H), 6.91 – 6.66 (m, 2H), 2.81 (t, *J* = 7.6 Hz, 4H), 1.64 (t, *J* = 7.6 Hz, 4H), 1.55 – 1.26 (m, 12H), 1.08 – 0.76 (m, 6H), ^{13}C NMR (75 MHz, DMSO-d_6) δ 169.39, 147.28, 137.45, 134.62, 131.58, 130.13 (CH), 127.20 (CH), 125.69 (CH), 31.52 (CH_2), 31.40 (CH_2), 29.81 (CH_2), 28.62 (CH_2), 22.47 (CH_2), 14.39 (CH_3), IR (ATR, cm^{-1}): v=403, 424, 449, 480, 522, 544, 569, 613, 635, 671, 723, 779, 787, 862, 887, 914, 962, 1010, 1051, 1124, 1209, 1238, 1288, 1317, 1400, 1427, 1464, 1502, 1685, 2524, 2634, 2856, 2923, 2962, 3070

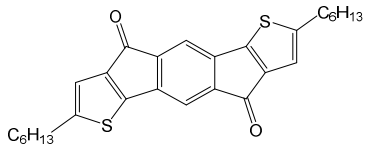

***para*-IDT(=O)$_2$**

2,7-dihexyl-s-indaceno[1,2-b:5,6-b']bisthiophene-4,9-dione

M.P.: 166-167°C (MeOH/CH_2Cl_2) ,^{1}H NMR (300 MHz, CD_2Cl_2) δ 7.06 (s, 2H), 6.78 – 6.74 (m, 2H), 2.84 – 2.72 (m, 4H), 1.74 – 1.61 (m, 4H), 1.39 – 1.27 (m, 12H), 0.96 – 0.83 (m, 6H), ^{13}C NMR (75 MHz, CD_2Cl_2) δ 186.13, 155.90, 151.86, 140.74, 139.84, 139.79, 117.82 (CH), 113.70 (CH), 31.47 (CH_2), 31.28 (CH_2), 30.53 (CH_2), 28.60 (CH_2), 22.55 (CH_2), 13.81 (CH_3), HRMS calculated for $C_{28}H_{31}O_2S_2$: 463.17655, Found: 463.1769 $[M+H]^+$, Elemental analysis calculated for $C_{28}H_{30}O_2S_2$: C, 72,69%; H, 6.54%, O, 6.92%, S, 13.86%. Found: C, 72.68%; H, 6.52%, O, 6.95 %, S, 13.68% IR (ATR, cm^{-1}): v=418, 442, 486, 561, 571, 596, 673, 723, 771, 814, 833, 862, 883, 916, 945, 976, 997, 1078, 1106, 1126, 1169, 1196, 1230, 1253, 1277, 1317, 1385, 1433, 1466, 1697, 2848, 2916, 2953, 3020, 3080, 3392

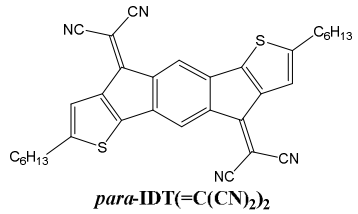

***para*-IDT(=C(CN)$_2$)$_2$**

2,2'-(2,7-dihexyl-s-indaceno[1,2-b:5,6-b']bisthiophene--4,9-diylidene)dipropanedinitrile

M.P.: N/A, ^{1}H NMR (300 MHz, 1,1,2,2-tetrachloroethane-D_2) δ 7.89 (s, 2H), 7.31 (s, 2H), 2.89 (t, J = 7.5 Hz, 4H), 1.91 – 1.67 (m, 4H), 1.48 (t, J = 7.3 Hz, 2H), 1.41 (d, J = 6.7 Hz, 10H), 1.12 – 0.88 (m, 6H), 13C NMR (75 MHz, 1,1,2,2-tetrachloroethane-D_2) δ: 155.65, 152.79, 150.66, 140.15, 139.40, 137.85, 119.62, 116.72, 112.71, 112.44, 31.20, 30.98, 30.67, 28.38, 22.25, 13.76., HRMS calculated for C_{34} H_{31} N_4 S_2: 559.19902, Found: 559.1995, Elemental analysis calculated for $C_{34}H_{30}N_4S_2$: C, 73.09%; H, 5.41%, N, 10.03%, S, 11.48%. Found: C, 72.10%, H, 5.22%, N, 9.83%, S, 11.50%, IR (ATR, cm^{-1}): v =403, 422, 434, 446, 469, 490, 526, 592, 663, 682, 692, 723, 739, 766, 793, 835, 890, 906, 1003, 1038, 1115, 1128, 1174, 1223, 1255, 1292, 1323, 1381, 1433, 1458, 1583, 1670, 1805, 2226, 2846, 2920, 2951, 3088

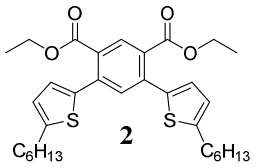

2

diethyl 4,6-bis(5-hexylthiophen-2-yl)isophthalate

Into a Schlenk tube containing anhydrous DMF (35 mL) was added diethyl 4,6-dibromoisophtalate (2.07g, 5.45 mmol, 1eq), 5-hexyl-2-tributylstannylthiophene (5.74g, 12.5mmol, 2.3 eq) and $Pd(PPh_3)_4$ (315 mg, 0.273 mmol, 0.05 eq). The mixture was stirred at 120°C under argon for 48 h. After the mixture was cooled to room temperature, water (150 mL) was added, and the aqueous layer was extracted with CH_2Cl_2 (3 x 100 mL). The combined organic layers were washed with water (3 x 200 mL), brine (1 x 200 mL), dried over $MgSO_4$ and evaporated using a rotary evaporator. The product was purified by flash chromatography with petroleum ether/CH_2Cl_2 (3/1 v/v) as eluent to afford **2** as an oil in a yield of 85% (2.57g, 4.65 mmol).

M.p. N/A, ^{1}H NMR (300 MHz, CD_2Cl_2) δ: 7.96 (d, J=0.46, 1H), 7.56 (s, 1H), 6.92 (d, *J* = 3.52 Hz, 2H), 6.76 (d, J=3.58, 2H), 4.23 (q, *J* = 7.14, 7.14, 7.15 Hz, 4H), 2.92 – 2.73 (m, 4H), 1.84 – 1.60 (m, 4H), 1.51 – 1.27 (m, 6H), 1.20 (t, *J* = 7.1 Hz, 12H), 1.04 – 0.77 (m, 6H), ^{13}C NMR (75 MHz, CD_2Cl_2) δ: 167.63, 147.94, 137.78, 136.59, 132.81 (CH), 130.63 (CH), 130.32, 126.88 (CH), 124.51 (CH), 61.44 (CH_2), 31.68 (CH_2), 31.53 (CH_2), 30.06 (CH_2), 28.75 (CH_2), 22.55 (CH_2), 13.79 (CH_3), 13.6 (CH_3), HRMS calculated for $C_{32}H_{42}O_4NaS_2$: 577.24167, Found: 577.2423 $[M+Na]^+$, IR (ATR, cm^{-1}): v = 802, 862, 1020, 1090, 1105, 1242, 1282, 1365, 1377, 1448, 1456, 1463, 1600, 1722, 2840, 2867, 2883, 2904, 2921, 2935, 2952, 2966, 2980

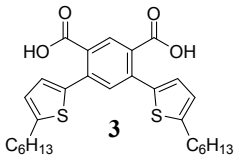

3

4,6-bis(5-hexylthiophen-2-yl)isophthalic acid

diethyl 4,6-bis(5-hexylthiophen-2-yl)isophthalate **2** (1.070g, 1.93 mmol, 1eq) and sodium hydroxide (309 mg, 7.72 mmol, 4 eq) were suspended in a mixture of ethanol (60 mL) and water (7 mL). The mixture was stirred at reflux overnight. About half of the solvent was evaporated before HCl 1N

(100mL) was added. The precipitate formed by the addition of HCl was filtrated, washed with water, and dried in the oven at 80°C, to afford a light grey solid in a yield of 62% (600 mg, 1.20 mmol).

M.p. 115°C, ^{1}H NMR (300 MHz, DMSO-d6) δ: 13.29 (s,2H), 7.82 (s, 1H), 7.47 (s, 1H), 7.08 (d, J = 3.5 Hz, 2H), 6.86 (dd, J = 3.6, 1.0 Hz, 2H), 2.81 (t, J = 7.6 Hz, 4H), 1.62 (q, J = 7.3 Hz, 4H), 1.40-1.25 (m, 12H), 0.94-0.82 (m, 6H),^{13}C NMR (75 MHz, CD_2Cl_2) δ: 169.15, 147.54, 137.57, 135.12, 131.89 (CH), 131.42, 129.91 (CH), 127.61 (CH), 125.63 (CH), 31.51 (CH_2), 31.39 (CH_2), 29.81 (CH_2), 28.61 (CH_2), 22.46 (CH_2), 14.36 (CH_3), HRMS calculated for $C_{28}H_{33}O_4S_2$: 497.18258, found: 497.1826 $[M-H]^-$, IR (ATR, cm^{-1}): v =413, 424, 438, 453, 469, 523, 538, 552, 571, 586, 644, 682, 722, 735, 769, 775, 800, 889, 921, 941, 1022, 1077, 1086, 1122, 1163, 1261, 1301, 1327, 1377, 1418, 1435, 1452, 1464, 1535, 1597, 1678, 1699, 1720, 2827, 2854, 2865, 2871, 2889, 2914, 2933, 2952, 2972, 3222.

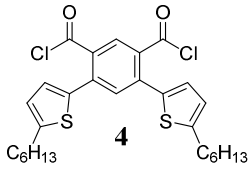

4

4,6-bis(5-hexylthiophen-2-yl)isophthaloyl dichloride

4,6-bis(5-hexylthiophen-2-yl)isophthalic acid **3** (450mg, 0.90 mmol, 1eq) and oxalyl chloride (1.243 g, 9.79 mmol, 10.9 eq) were suspended in dry CH_2Cl_2 (15 mL) with several drop of DMF and the mixture was stirred overnight at room temperature. The solvent was evaporated under vacuum to obtain the crude acid dichloride **4** which was used for the next step without further purification.

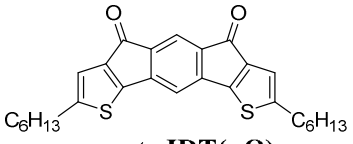

***meta*-IDT(=O)$_2$**

2,8-dihexyl-*s*-indaceno[1,2-*b*:7,6-*b*']dithiophene-4,6-dione

Aluminium chloride (341mg, 2.56 mmol, 2.8 eq) was suspended in dry CH_2Cl_2 (15 mL) and cooled at 0°C. 4,6-bis(5-hexylthiophen-2-yl)isophthalic acid dichloride **4** was dissolved in CH_2Cl_2 (15 mL) and the mixture was cooled at 0°C. The latter was slowly added to the aluminium chloride in CH_2Cl_2 at 0°C and stirred for 20 min at this temperature then overnight at room temperature. Water with 1M HCl were added and the product was extracted with CH_2Cl_2. The organic phase was dried over $MgSO_4$ and evaporated and the product was reprecipitated in a mixture composed of the minimum amount of CH_2Cl_2 in MeOH. The solid was filtrated and dried under vacuum, giving a brown powder of ***meta*-IDT(=O)$_2$** in a yield of 86% (360 mg, 0.78 mmol).

M.p. 141°C (DCM/MeOH),^{1}H NMR (300 MHz, CD_2Cl_2) δ: 7.32 (d, J = 0.7 Hz, 1H), 6.84 (d, J = 0.7 Hz, 1H), 6.82 – 6.80 (m, 2H), 2.81 (d, J = 7.5 Hz, 4H), 1.75 – 1.64 (m, 4H), 1.46 – 1.22 (m, 12H), 0.89 (d, J = 6.7 Hz, 6H),^{13}C NMR (75 MHz, CD_2Cl_2) δ 186.10, 154.03, 153.86, 146.85, 143.25, 134.28, 118.58 (CH), 118.11 (CH), 110.65 (CH), 31.90 (CH_2), 31.73 (CH_2), 31.08 (CH_2), 29.03 (CH_2), 22.98 (CH_2), 14.23 (CH_3), HRMS calculated for $C_{28}H_{30}O_2S_2$: 463.17655, found: 463.1766 $[M+H]^+$, Elemental analysis calculated for $C_{28}H_{30}O_2S_2$: C, 72,69%; H, 6.54%, O, 6.92%, S, 13.86%. Found: C, 72.42%; H, 6.46%, O, 7.06 %, S, 13.72%, IR (ATR, cm^{-1}): v =438, 476, 507, 552, 572, 717, 775, 804, 831, 903, 985, 1003, 1074, 1126, 1169, 1236, 1317, 1369, 1398, 1429, 1456, 1514, 1589, 1693, 1786, 2854, 2926, 2954, 3085.

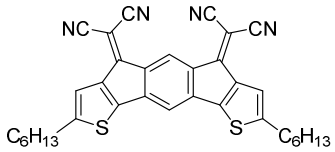

***meta*-IDT(=C(CN)$_2$)$_2$**

2,2'-(2,8-dihexyl-s-indaceno[1,2-*b*:7,6-*b*']dithiophene-4,6-diylidene)dimalononitrile

2,8-dihexyl-s-indaceno[1,2-b:7,6-b']dithiophene-4,6-dione, ***meta*-IDT(=O)$_2$**, (200mg, 0.44 mmol, 1 eq), malononitrile (84 mg, 1.27 mmol, 2.88 eq) and pyridine (1.96 g, 24.8 mmol, 112.7 eq) were dissolved in dry CH_2Cl_2 (30mL) and the mixture was stirred overnight at 30°C. The crude product was filtrated and reprecipitated in the minimum amount of hot chlorobenzene giving a brown powder in a yield of 82% (203 mg, 0.36 mmol).

M.p. N/A, ^{1}H NMR (300 MHz, 1,1,2,2-tetrachloroethane-D2) δ: 8.77 (s, 1H), 7.41 (d, J = 1.0 Hz, 2H), 7.08 (s, 1H), 2.93 (t, J = 7.5 Hz, 4H), 1.78 (q, J = 7.4 Hz, 4H), 1.41 (m, J = 7.5, 3.8 Hz, 12H), 1.03 – 0.93 (m, 6H), ^{13}C NMR (75 MHz, 1,1,2,2-tetrachloroethane-D_2) δ: 155.42, 154.94, 147.90, 144.25, 142.29, 133.05, 122.45, 120.23, 113.07, 112.22, 111.32, 31.20, 31.03, 30.85, 28.41, 22.26, 13.76.; HRMS calculated for $C_{34}H_{30}N_4NaS_2$: 581.1804, found: 581.1803 $[M+Na]^+$, Elemental analysis calculated for $C_{34}H_{30}N_4S_2$: C, 73.09%; H, 5.41%, N, 10.03%, S, 11.48%. Found: C, 71.86%; H, 5.31%, N, 9.81%, S, 11.38%, IR (ATR, cm^{-1}): v = 432, 472, 490, 511, 594, 629, 671, 714, 758, 793, 835, 893, 978, 1036, 1066, 1111, 1134, 1178, 1225, 1240, 1261, 1324, 1376, 1398, 1434, 1461, 1556, 1599, 1668, 1783, 2221, 2846, 2870, 2919, 2950, 3039, 3095

THERMAL PROPERTIES: TGA, DSC & SWAX

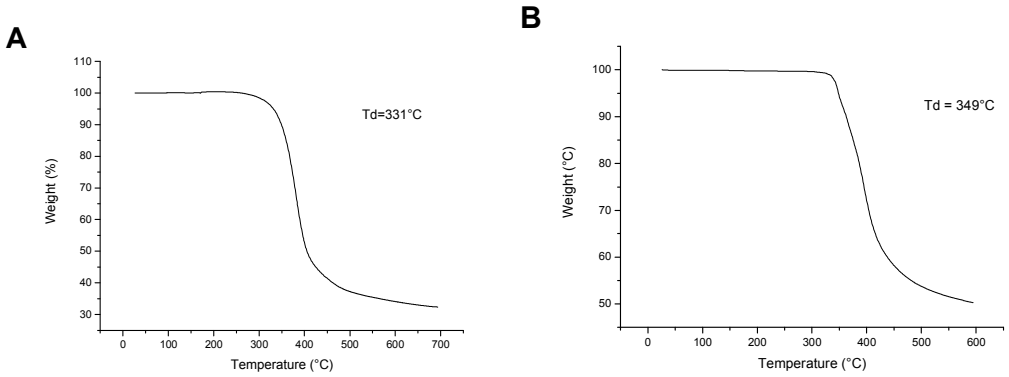

Figure S1 : TGA of ***para*-IDT(=O)$_2$** (**A**) and ***para*-IDT(=C(CN)$_2$)$_2$** (**B**)

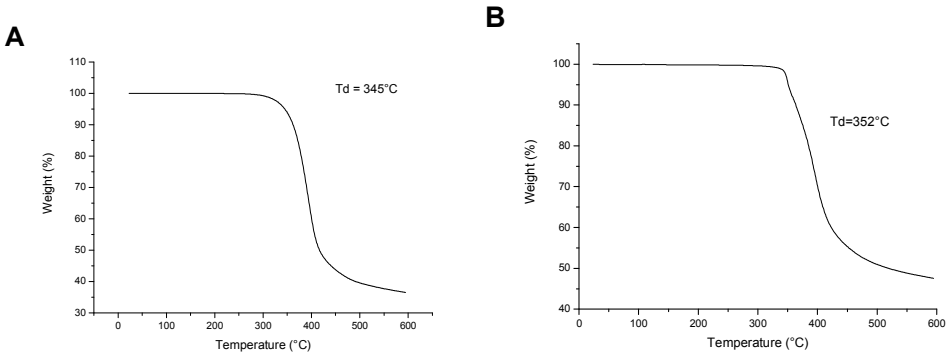

Figure S2 : TGA of ***meta*-IDT(=O)$_2$** (**A**) and ***meta*-IDT(=C(CN)$_2$)$_2$** (**B**)

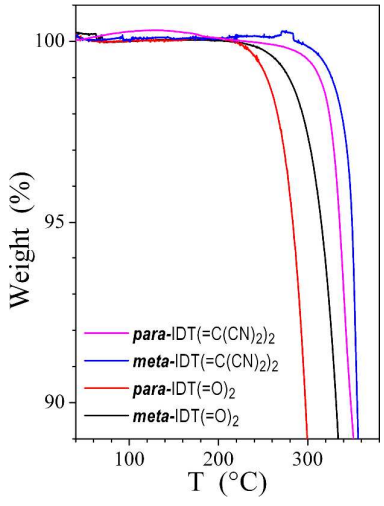

Figure S3 : Comparison of the TGA recorded for ***meta*-IDT(=O)$_2$** (grey) or ***para*-IDT(=O)$_2$** (red) and ***meta*-IDT(=C(CN)$_2$)$_2$** (blue) or ***para*-IDT(=C(CN)$_2$)$_2$** (pink)

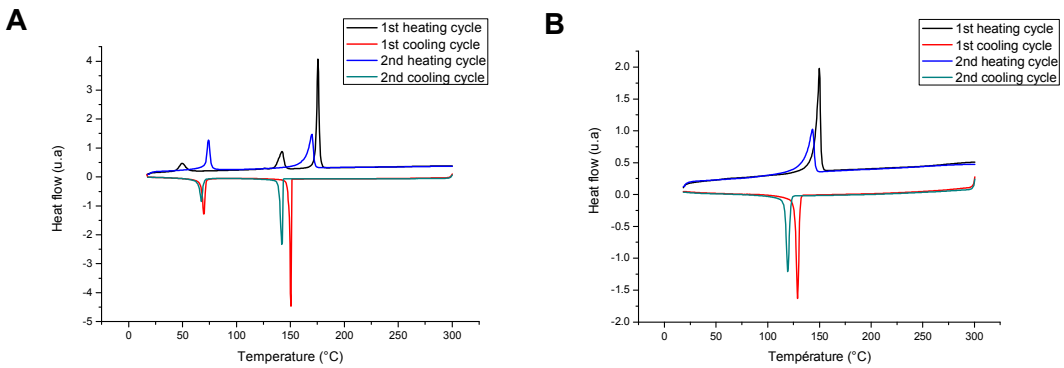

Figure S4 :DSC of ***para*-IDT(=O)$_2$** (**A**) and ***meta*-IDT(=O)$_2$** (**B**)

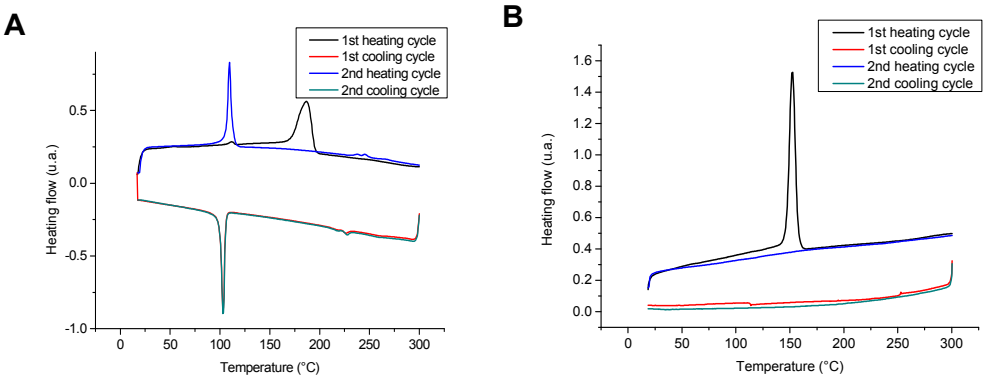

Figure S5 : DSC of ***para*-IDT(=C(CN)$_2$)$_2$** (**A**) and ***meta*-IDT(=C(CN)$_2$)$_2$** (**B**)

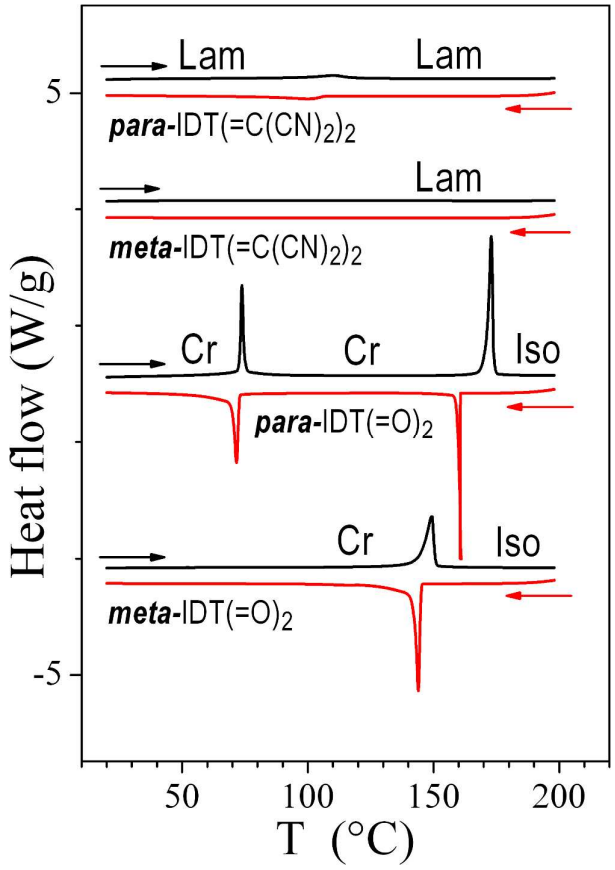

Figure **S6**. DSC traces of $IDT(=O)_2$ and $IDT(=C(CN)_2)_2$ regioisomers (2^{nd} heating run (black) and cooling run (re) at 5°C/min, endotherm up); Cr: crystalline phase; Iso: isotropic liquid, Lam: three-dimensional lamellar mesophase.

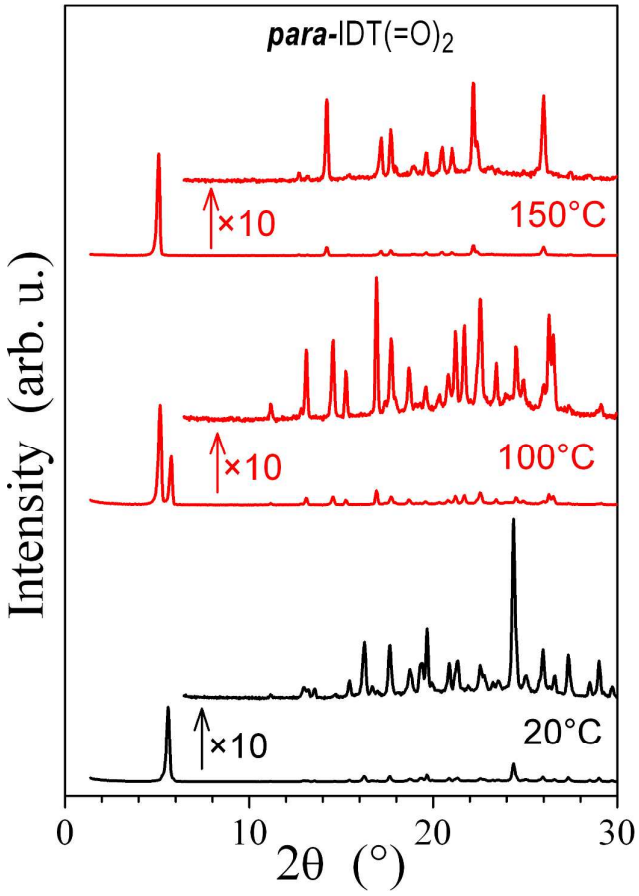

Figure **S7**. SWAXS patterns of sequence of crystalline phases of ***para*-IDT(=C(CN)$_2$)$_2$**, at room temperature in the pristine state (bottom, black) and on first heating (middle and top, red).

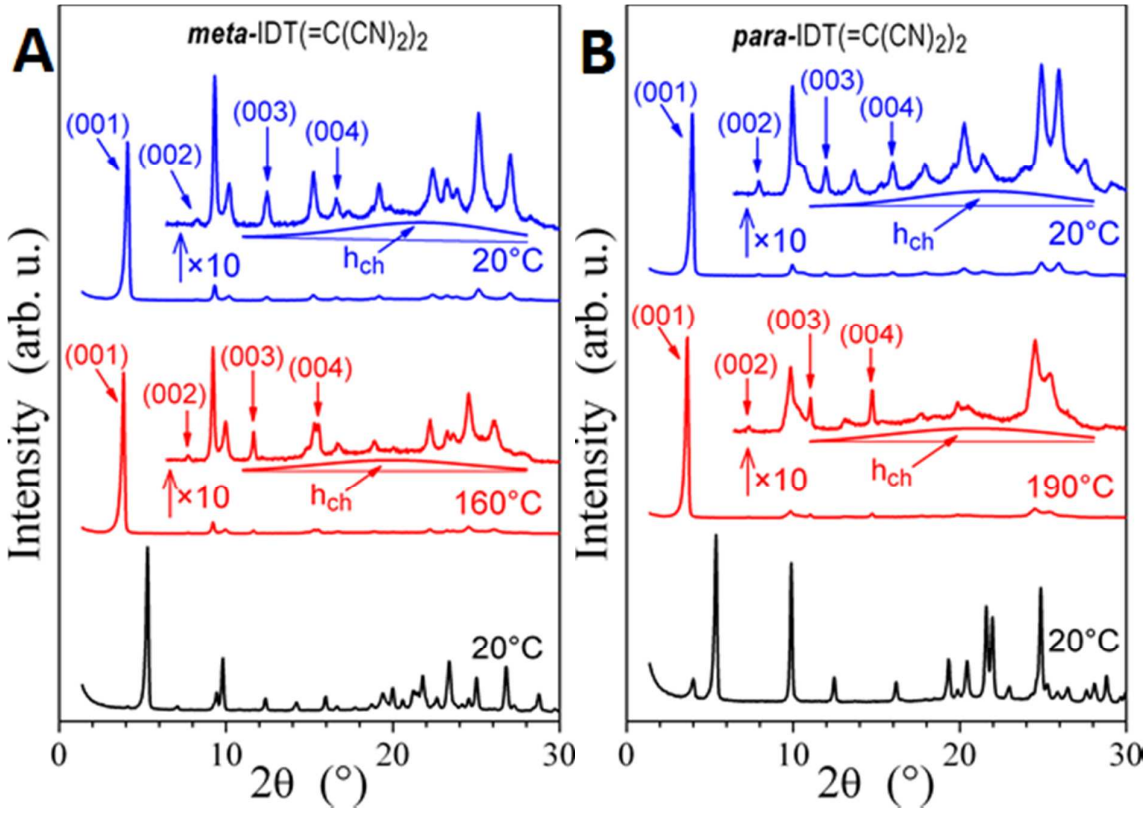

Figure S8: SWAXS patterns of ***meta*-IDT(=C(CN)$_2$)$_2$** (A) and of ***para*-IDT(=C(CN)$_2$)$_2$** (B), at room temperature in the pristine state (bottom, black), above the melting to a three-dimensional lamellar mesophase (middle, red) and on cooling at room temperature, in a frozen state of the lamellar mesophase (top, blue); h_{ch} is the scattering signal for molten alkyl chains, the lamellar reflections series is identified by indexations (00/).

PHOTOPHYSICAL PROPERTIES

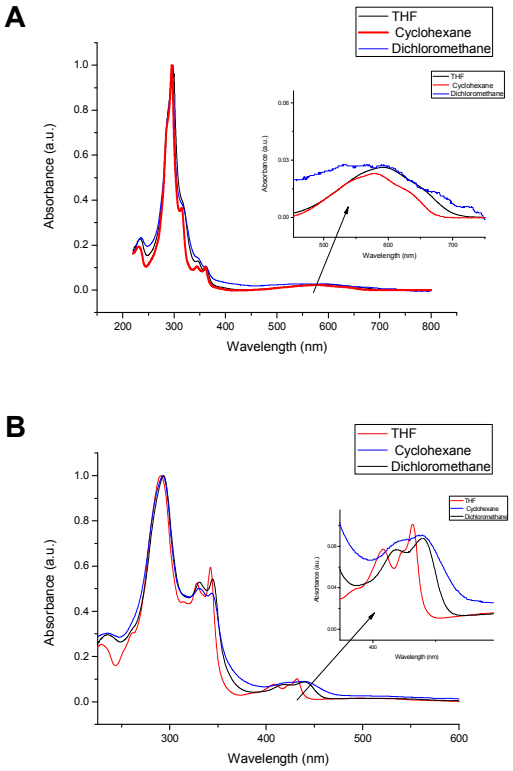

Figure S9. Comparison of absorption spectra of ***para*-IDT(=O)$_2$** (**A**) and ***meta*-IDT(=O)$_2$** (**B**) in different solvents, C = 10^{-6}M

THEORETICAL MODELING

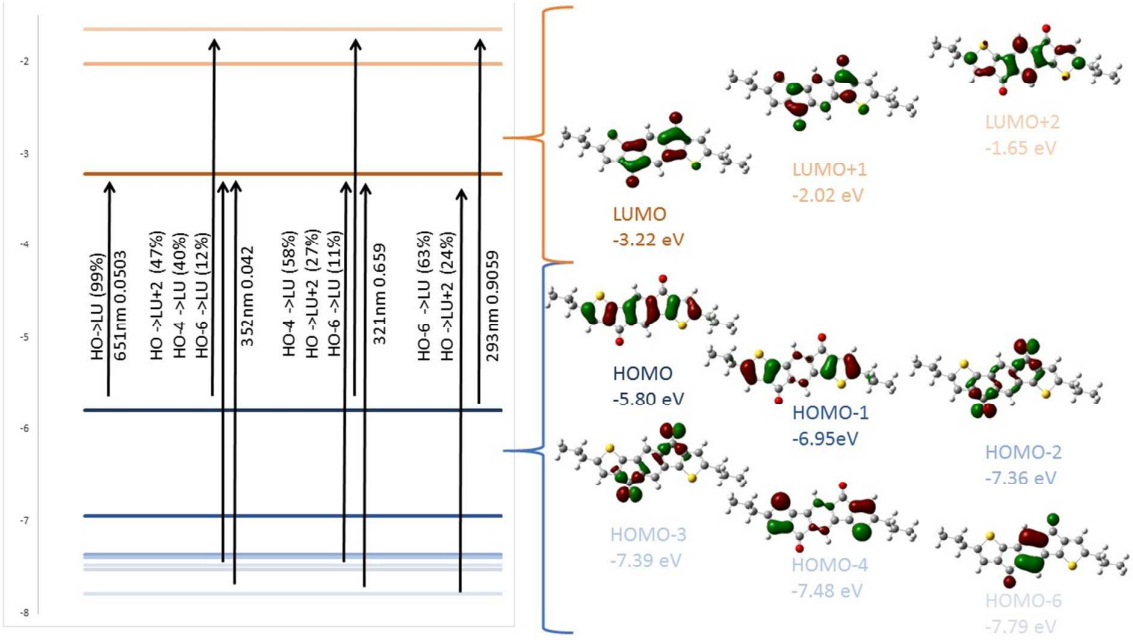

Figure S10. Calculated frontier molecular orbitals by DFT and four electronic transitions of interest calculated by TD-DFT of ***para*-IDT(=O)$_2$**, after geometry optimization with DFT B3LYP/6-311G+(d,p), shown with a cut-off 0.04

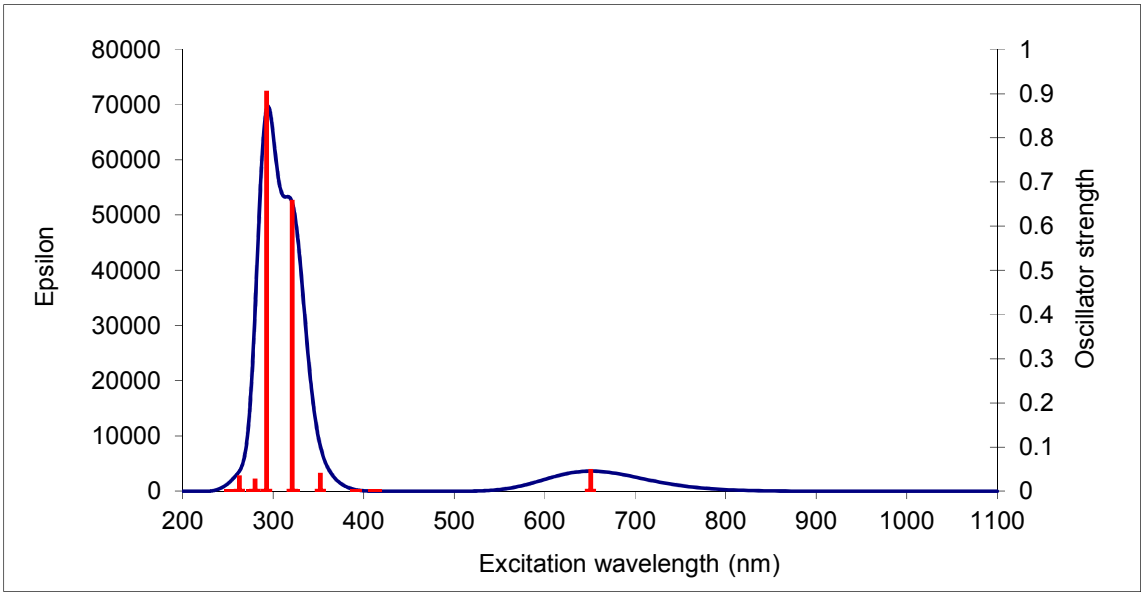

Figure S11. Predicted UV-vis spectra from TD-DFT energy calculations of ***para*-IDT(=O)$_2$** after geometry optimization with DFT B3LYP/6-311 G+(d,p).

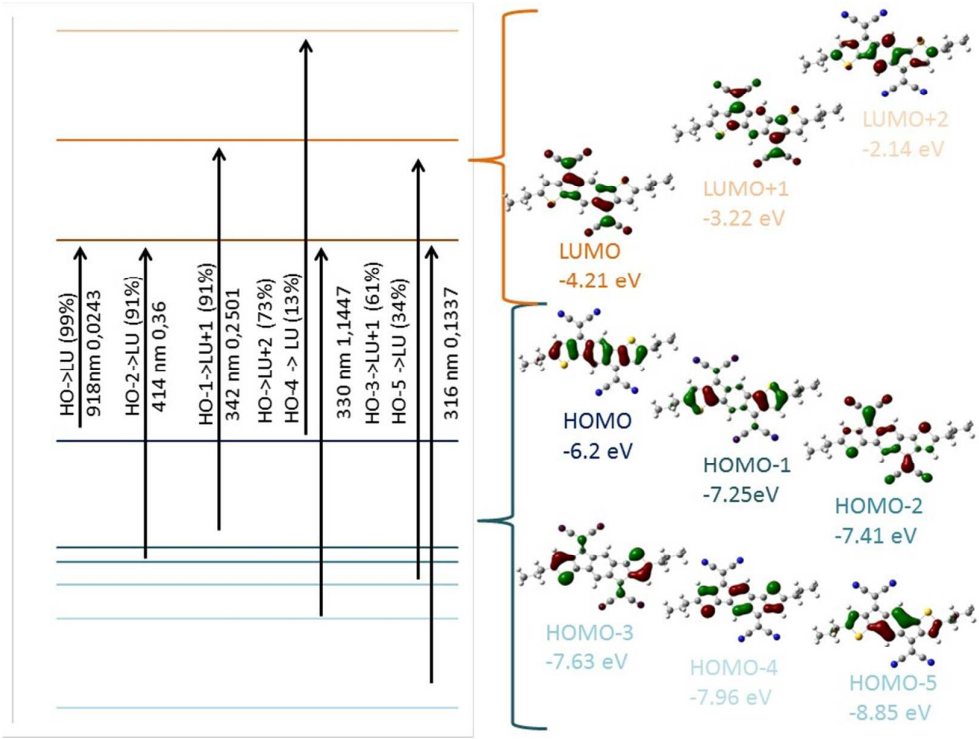

Figure S12. Calculated frontier molecular orbitals by DFT and five electronic transitions of interest calculated by TD-DFT of ***para*-IDT(=C(CN)$_2$)$_2$**, after geometry optimization with DFT B3LYP/6-311G+(d,p), shown with a cut-off 0.04

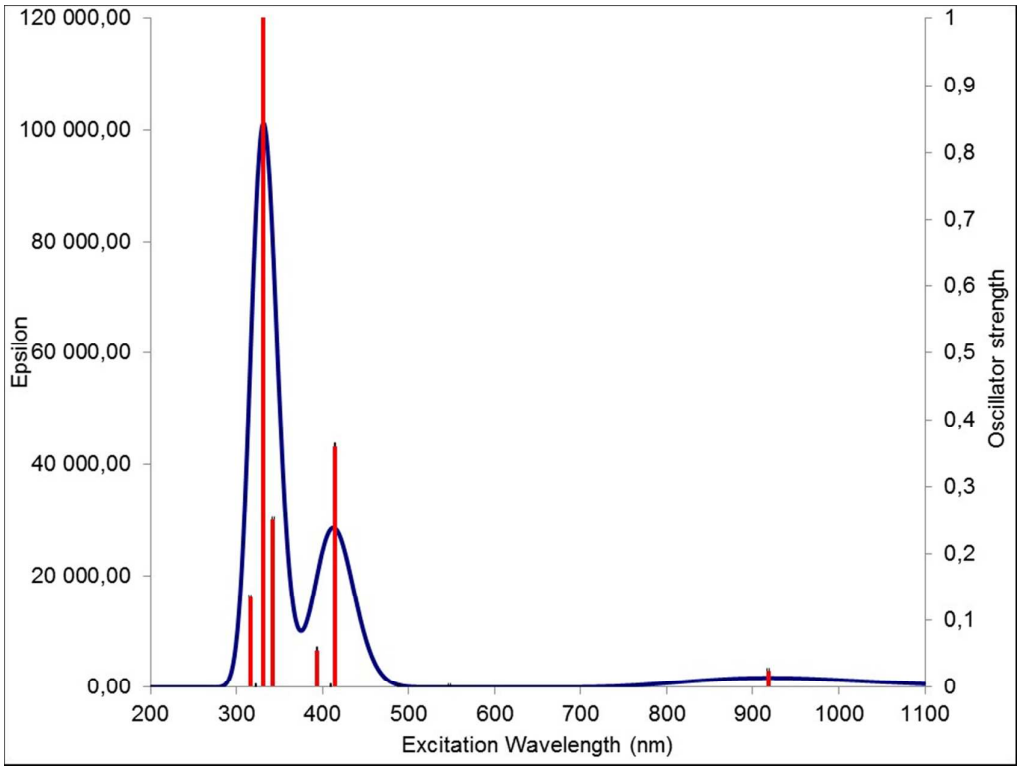

Figure S13. Predicted UV-vis spectra from TD-DFT energy calculations of ***para*-IDT(=C(CN)$_2$)$_2$** after geometry optimization with DFT B3LYP/6-311 G+(d,p).

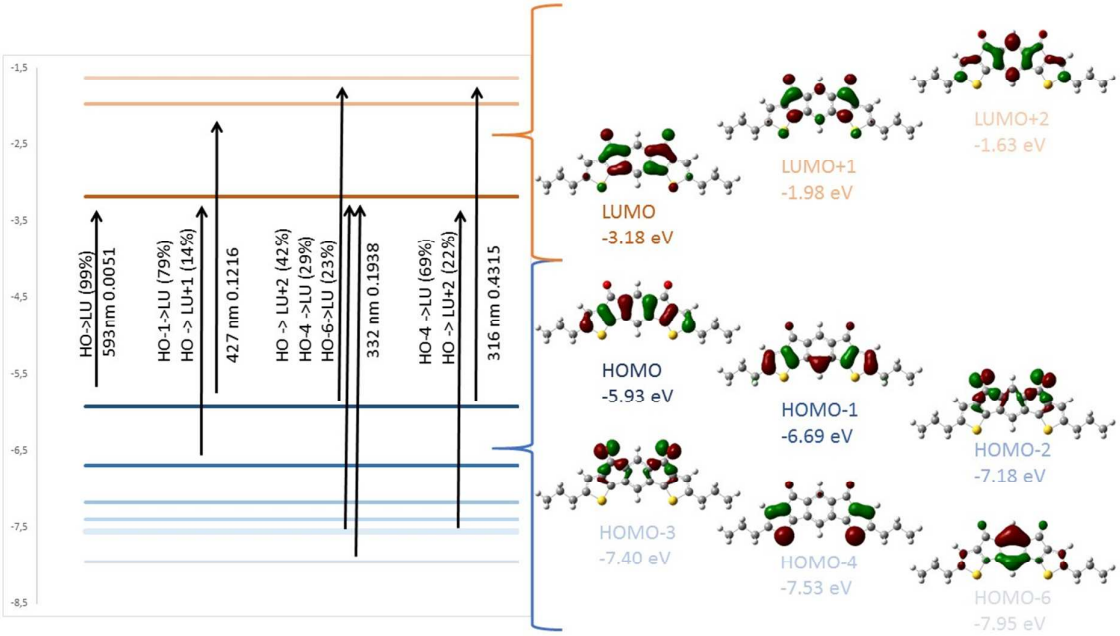

Figure S14. Calculated frontier molecular orbitals by DFT and four electronic transitions of interest calculated by TD-DFT of ***meta*-IDT(=O)$_2$**, after geometry optimization with DFT B3LYP/6-311G+(d,p), shown with a cut-off 0.04

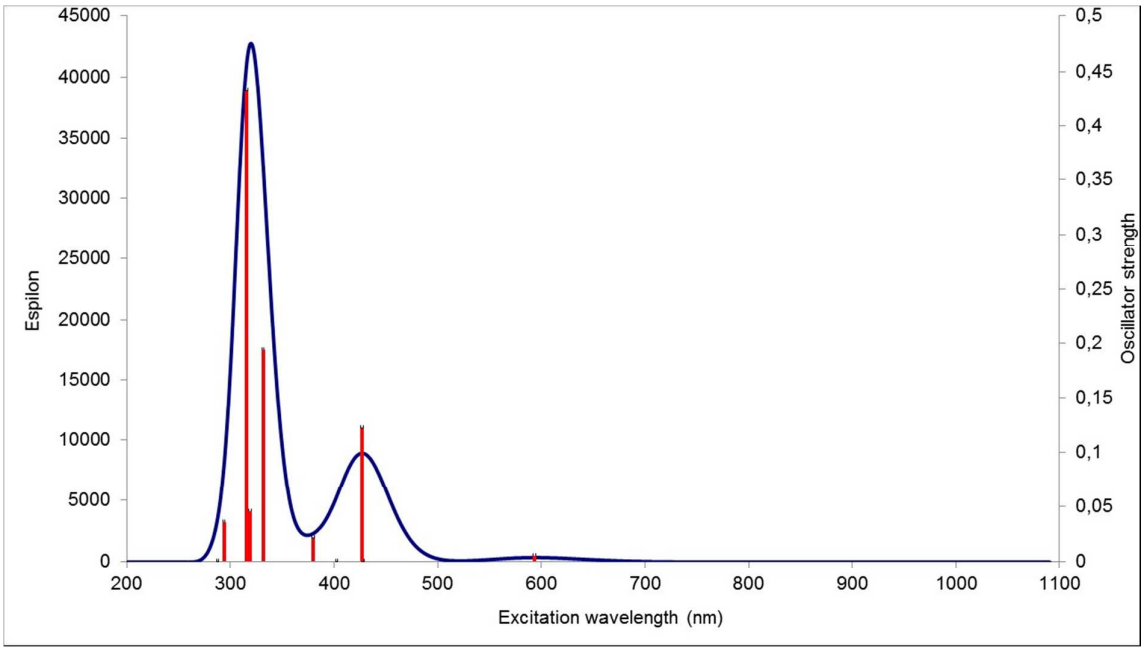

Figure S15. Predicted UV-vis spectra from TD-DFT energy calculations of ***meta*-IDT(=O)$_2$** after geometry optimization with DFT B3LYP/6-311 G+(d,p).

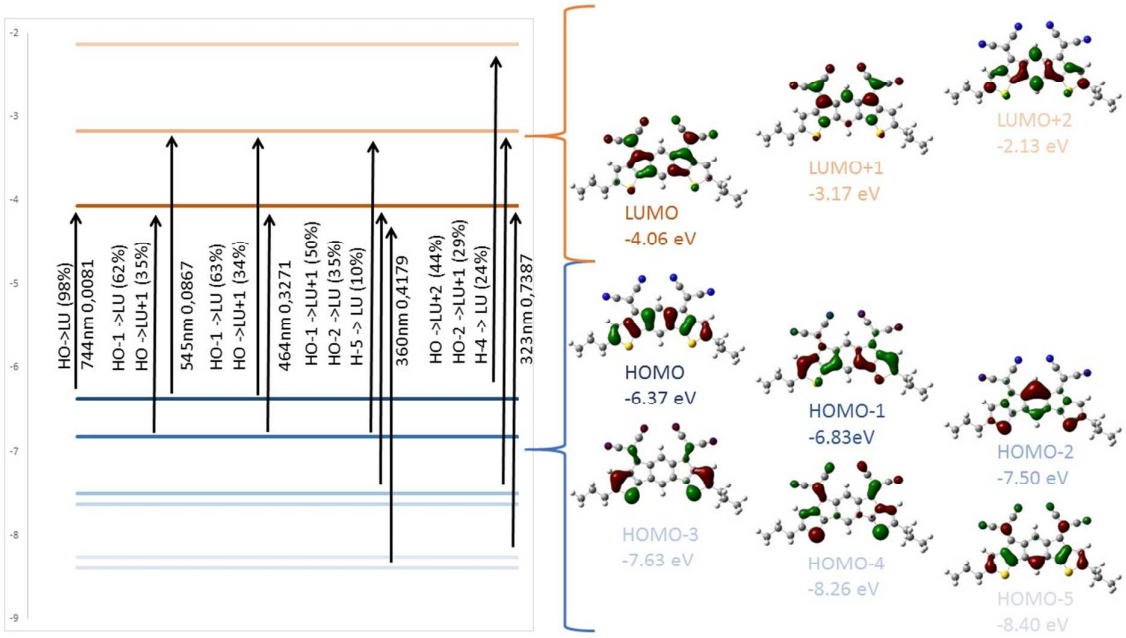

Figure S16. Calculated frontier molecular orbitals by DFT and five electronic transitions of interest calculated by TD-DFT of ***meta*-IDT(=C(CN)$_2$)$_2$**, after geometry optimization with DFT B3LYP/6-311G+(d,p), shown with a cut-off 0.04

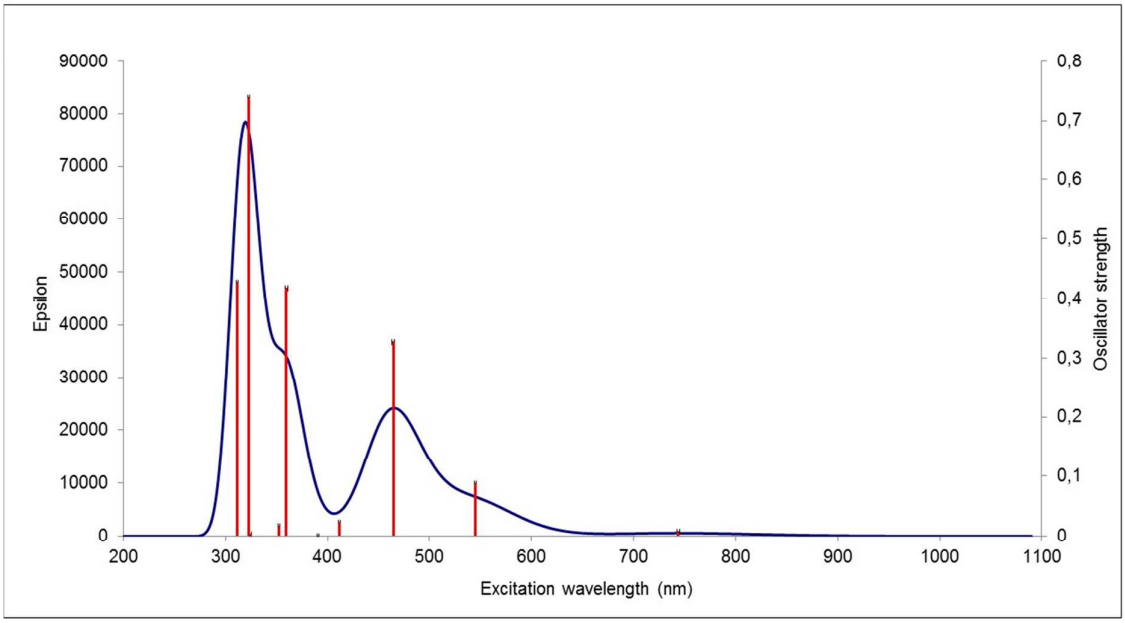

Figure S17. Predicted UV-vis spectra from TD-DFT energy calculations of ***meta*-IDT(=C(CN)$_2$)$_2$** after geometry optimization with DFT B3LYP/6-311 G+(d,p).

ORGANIC FIELD-EFFECT TRANSISTORS STRUCTURE AND FABRICATION

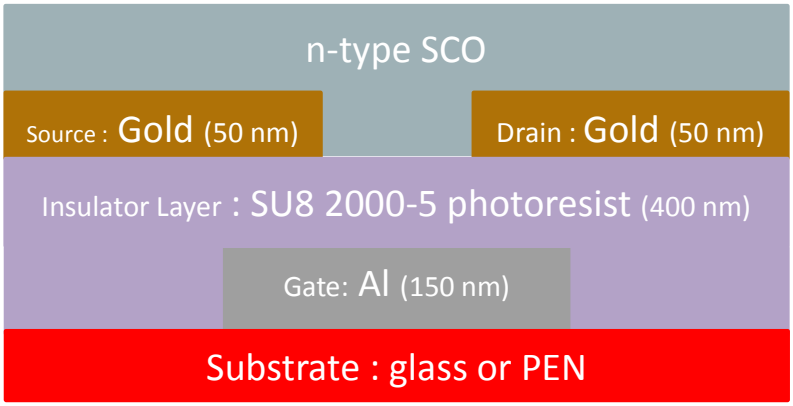

Figure S18. Structure of the OFETs : on glass or PEN substrate

The fabrication process is described as follows: 150 nm thick aluminium layer was evaporated and patterned by conventional photolithography on a 5x5 cm^2 rigid glass substrate or on flexible polyethylene naphtalate (PEN) substrate. Then, SU-8 2000.5 Photoresist from Microchem[10] was then spin-coated in order to obtain a 400 nm thick layer. 50 nm thick gold layer was then thermally evaporated and patterned by photolithography. Finally, the OSCs were deposited by evaporation under vacuum as a 40 nm thick layer.

SAMS deposition :

After the gold electrodes photolithography, the substrates were immerged in a solution of DABT (4-(dimethylamino)benzenethiol) in acetone (10 mg/mL) for 10 minutes at room temperature without stirring. The substrates were then rinsed with acetone and used for the active layer evaporation under vacuum.

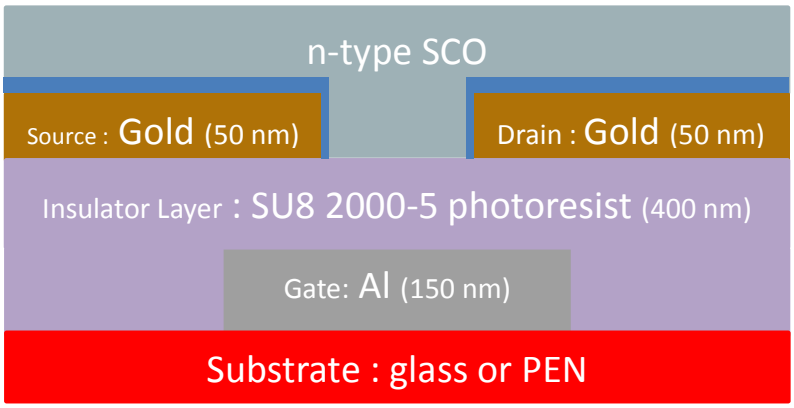

Figure S19. Structure of the OFETs with modified electrodes (DABT layer in blue on source and drain electrodes).

In both cases, the OSCs have been deposited in the last step of the fabrication process avoiding any external effect on the OSC materials.[11-13]

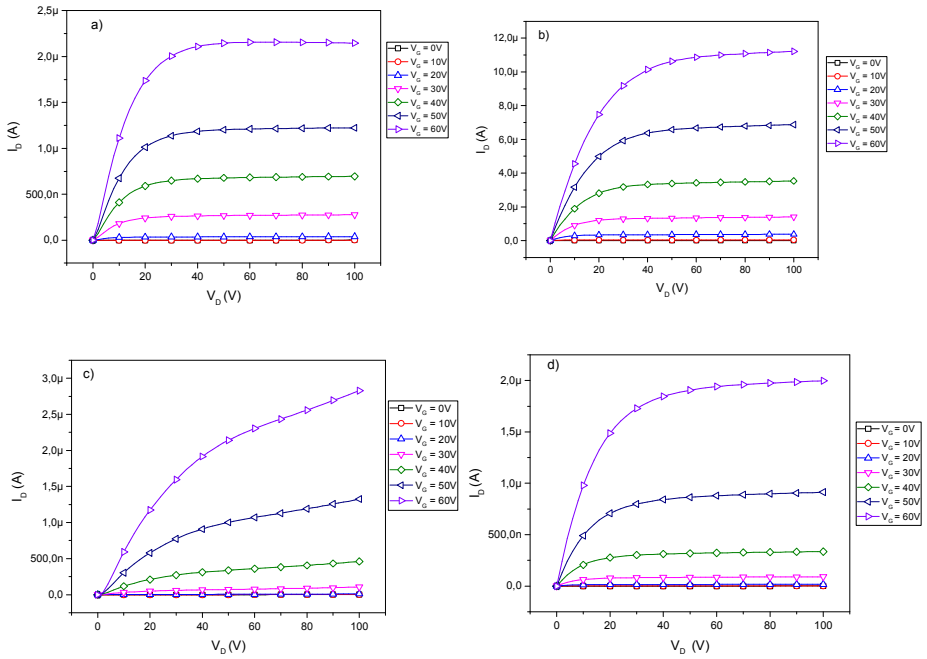

Figure S20: Output characteristics of OFETs on glass with ***para*-IDT(=C(CN)$_2$)$_2$** without DABT (a) and with DABT (b) and ***meta*-IDT(=C(CN)$_2$)$_2$** without DABT (c) and with DABT (d)

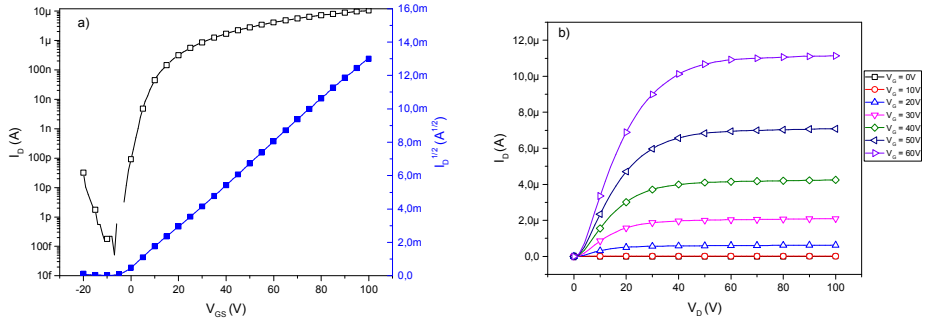

Figure S21: Transfer characteristics (a) and output characteristics (b) of OFETs with *para*-IDT(=C(CN)$_2$)$_2$ on PEN without DABT.

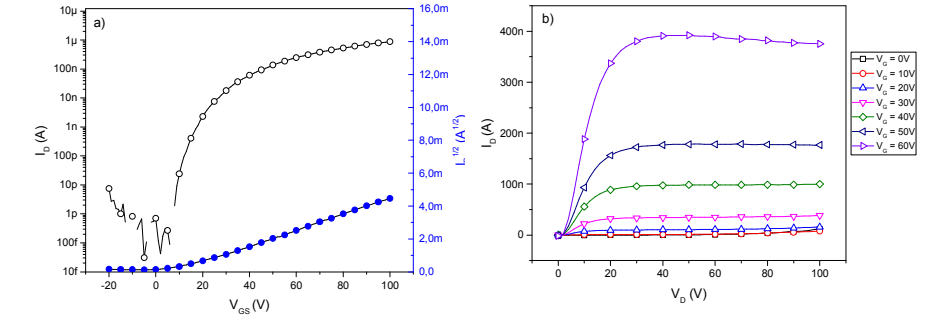

Figure S22: Transfer characteristics (a) and output characteristics (b) of OFETs with *meta*-IDT(=C(CN)$_2$)$_2$ on PEN without DABT.

2D NMR STUDIES

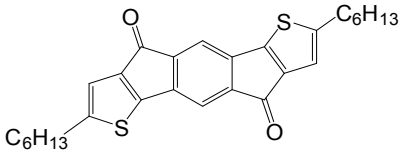

***Para*-IDT(=O)$_2$**

COSY-CD_2Cl_2

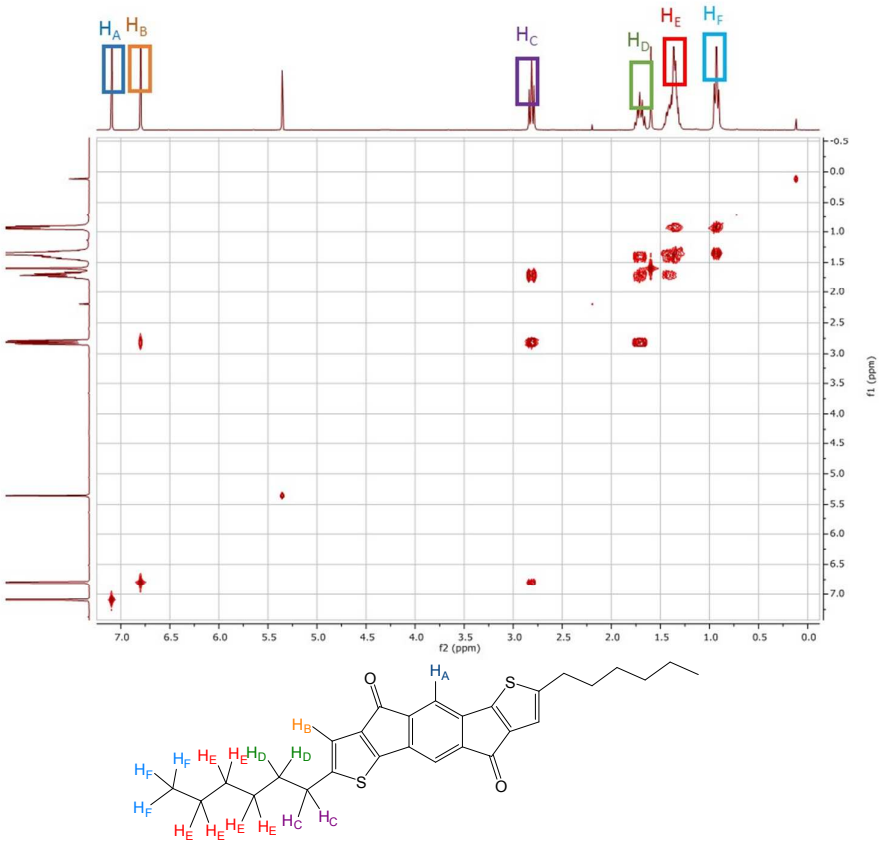

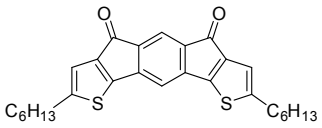

***meta*-IDT(=O)$_2$**

2,8-dihexyl-*s*-indaceno[1,2-*b*:7,6-*b*']dithiophene-4,6-dione

COSY-CD_2Cl_2

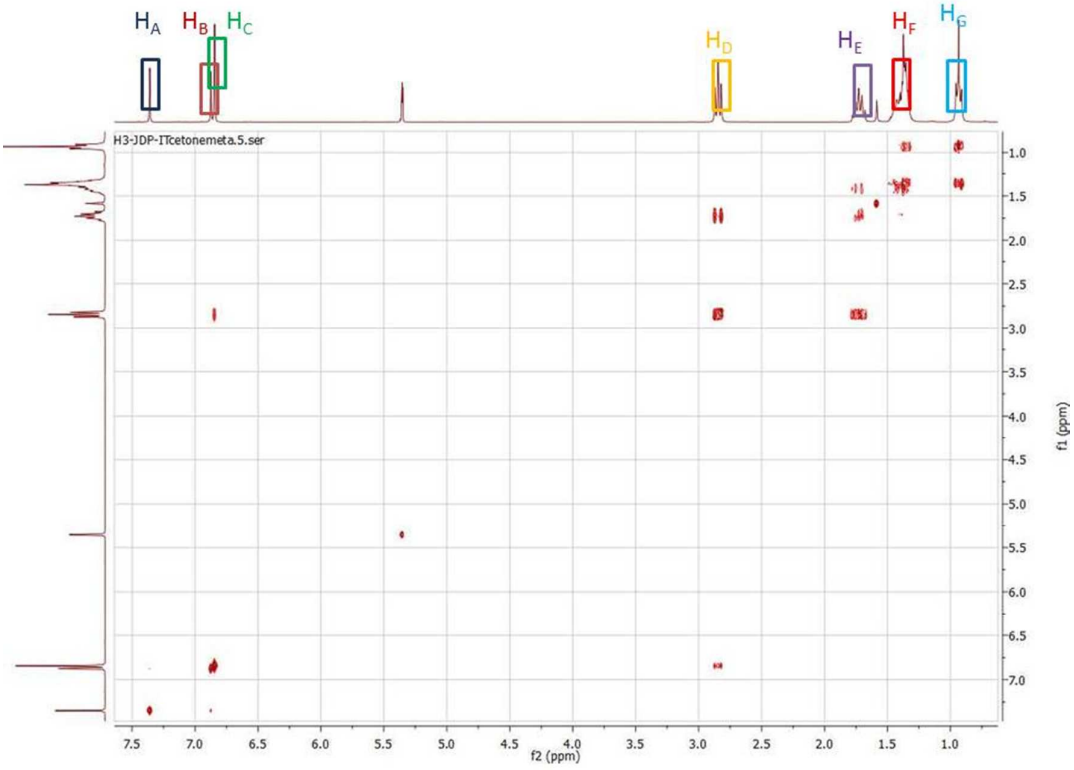

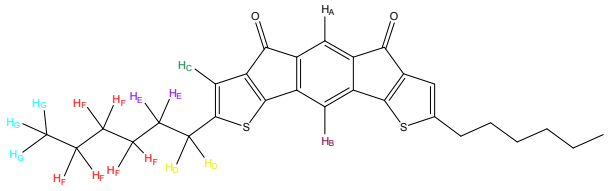

Copies of the different NMR spectra

diethyl 2,5-bis(5-hexylthiophen-2-yl)benzene-1,4-dicarboxylate

^{1}H NMR in CD_2Cl_2

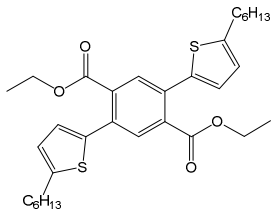

diethyl 2,5-bis(5-hexylthiophen-2-yl)benzene-1,4-dicarboxylate

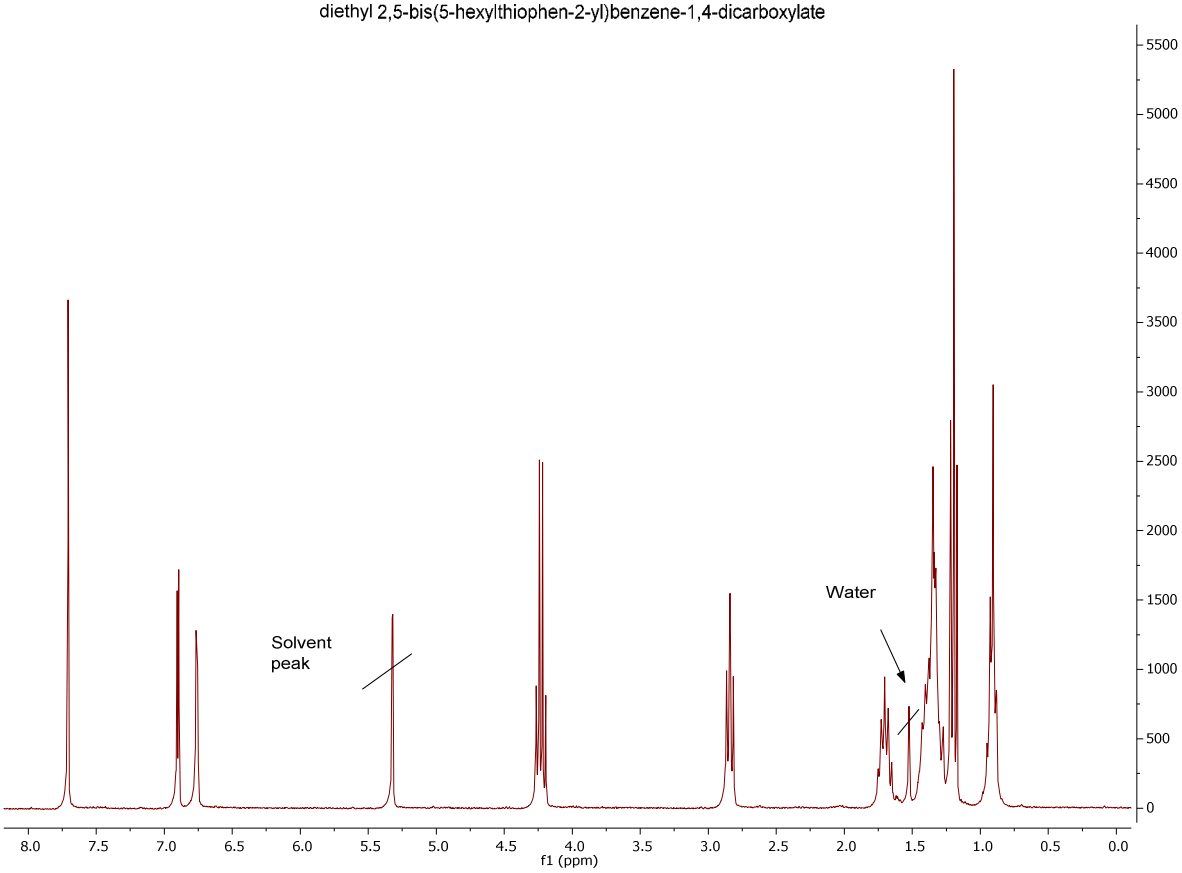

2,5-bis(5-hexylthiophen-2-yl)benzene-1,4-dicarboxylic acid

^{1}H NMR in DMSO

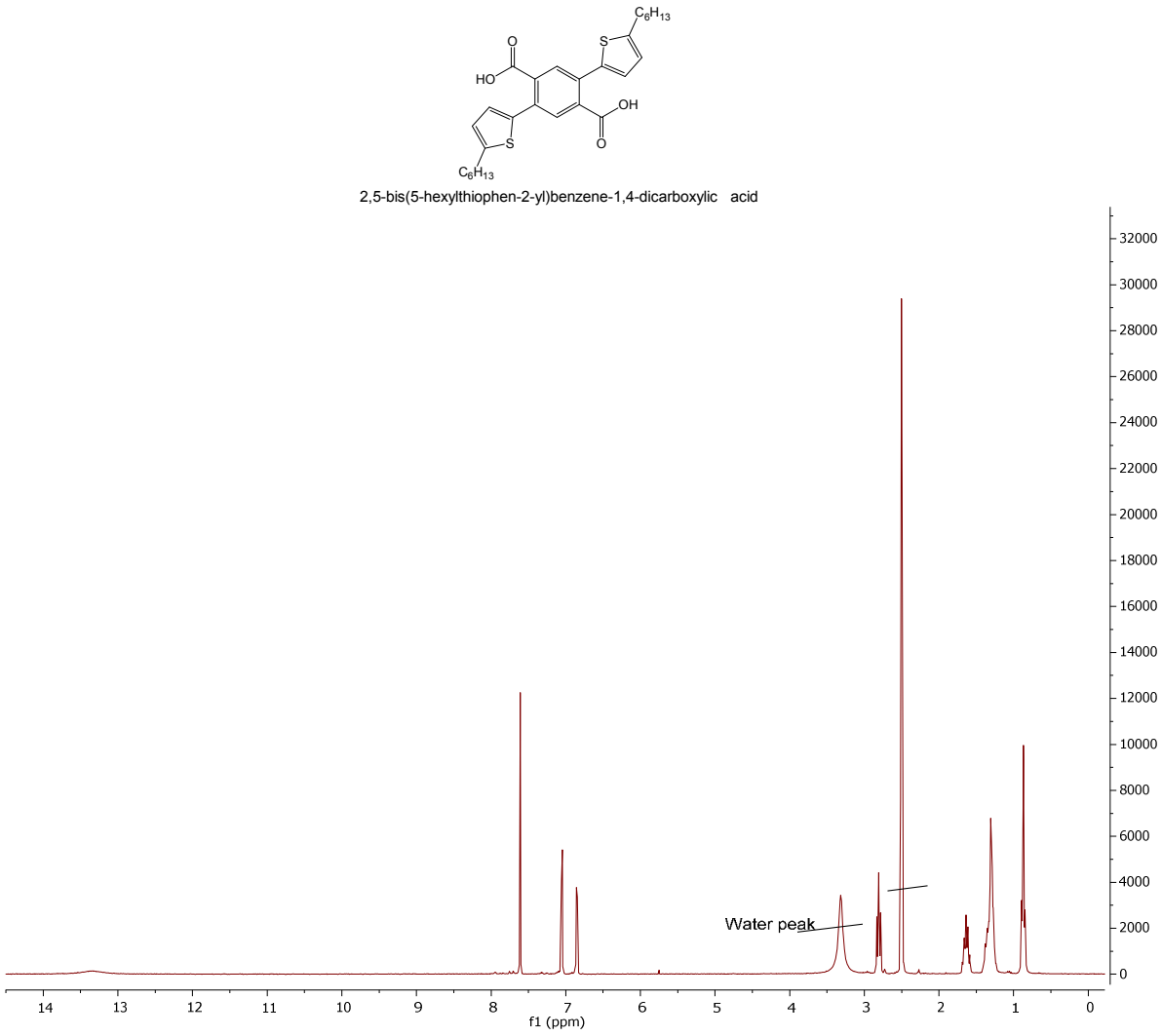

2,5-bis(5-hexylthiophen-2-yl)benzene-1,4-dicarboxylic acid

^{13}C NMR in DMSO

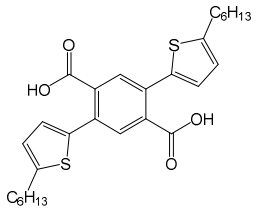

2,5-bis(5-hexylthiophen-2-yl)benzene-1,4-dicarboxylic acid

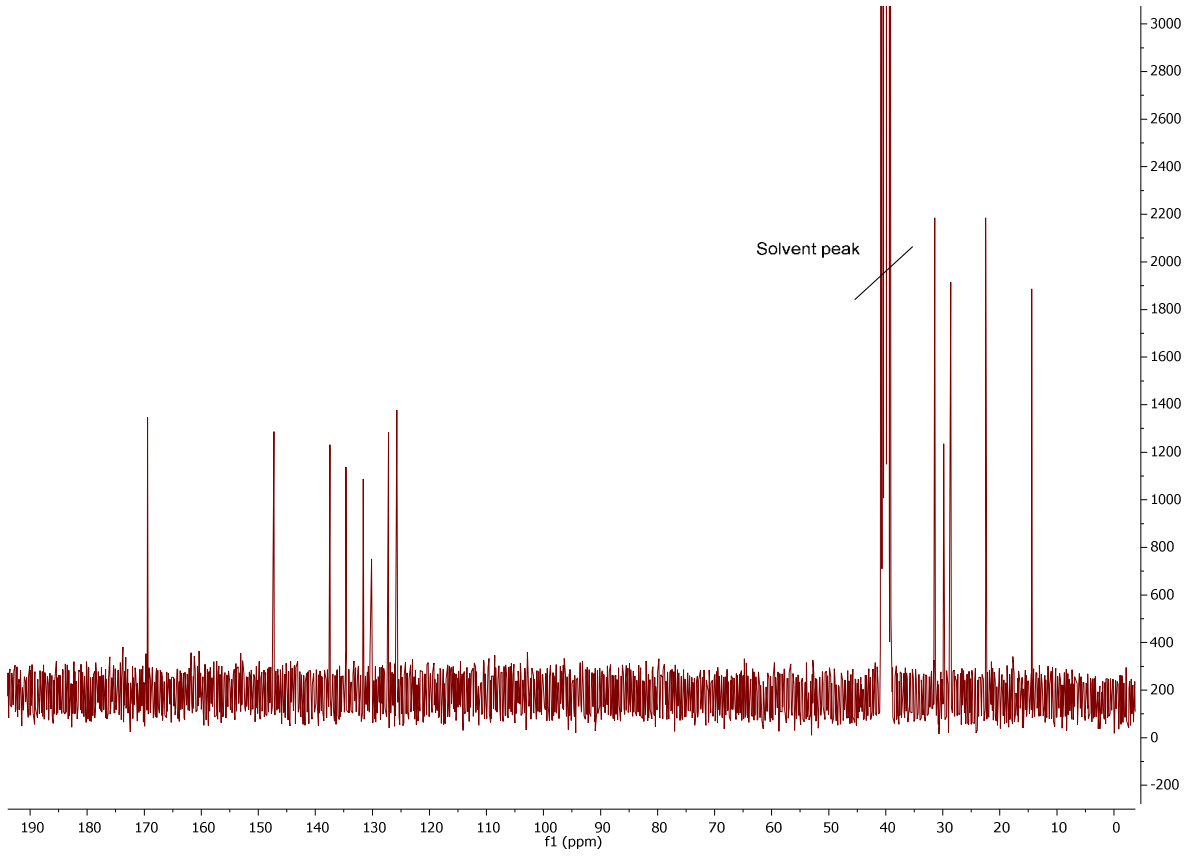

2,5-bis(5-hexylthiophen-2-yl)benzene-1,4-dicarboxylic acid

DEPT in DMSO

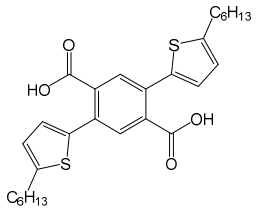

2,5-bis(5-hexylthiophen-2-yl)benzene-1,4-dicarboxylic acid

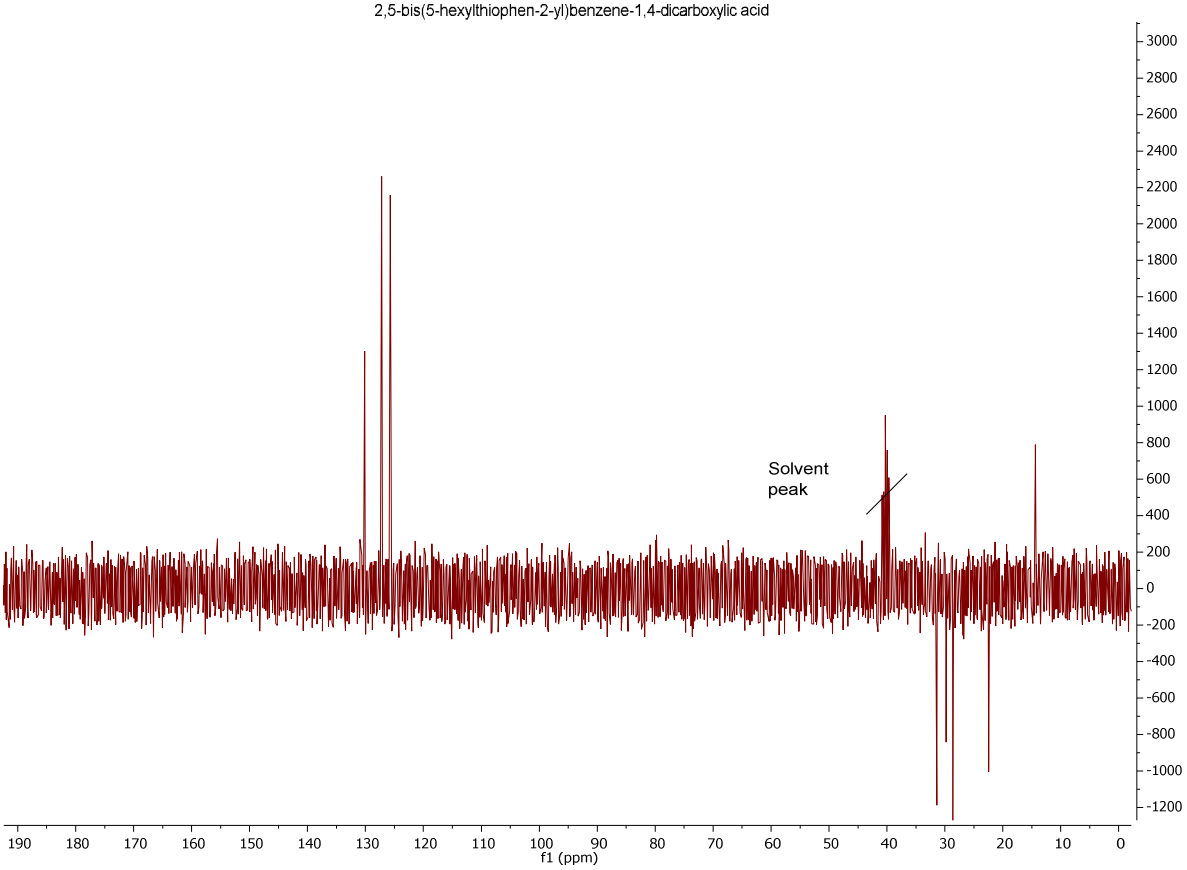

2,7-dihexyl-s-indaceno[1,2-b:5,6-b']bisthiophene-4,9-dione

^{1}H NMR in CD_2Cl_2

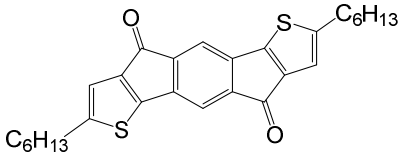

***Para*-IDT(=O)$_2$**

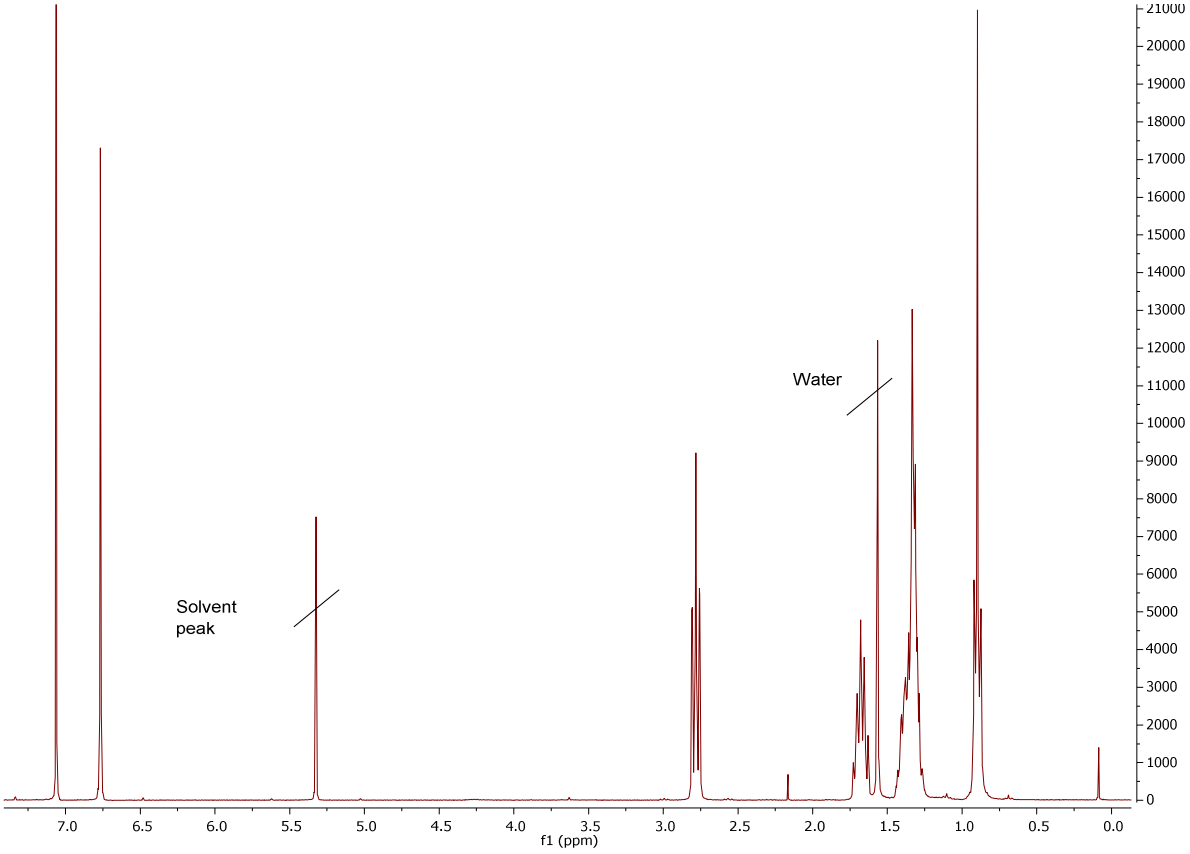

2,7-dihexyl-s-indaceno[1,2-b:5,6-b']bisthiophene-4,9-dione

^{13}C NMR in CD_2Cl_2

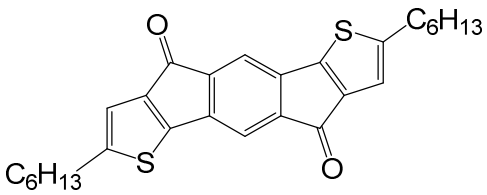

***Para*-IDT(=O)$_2$**

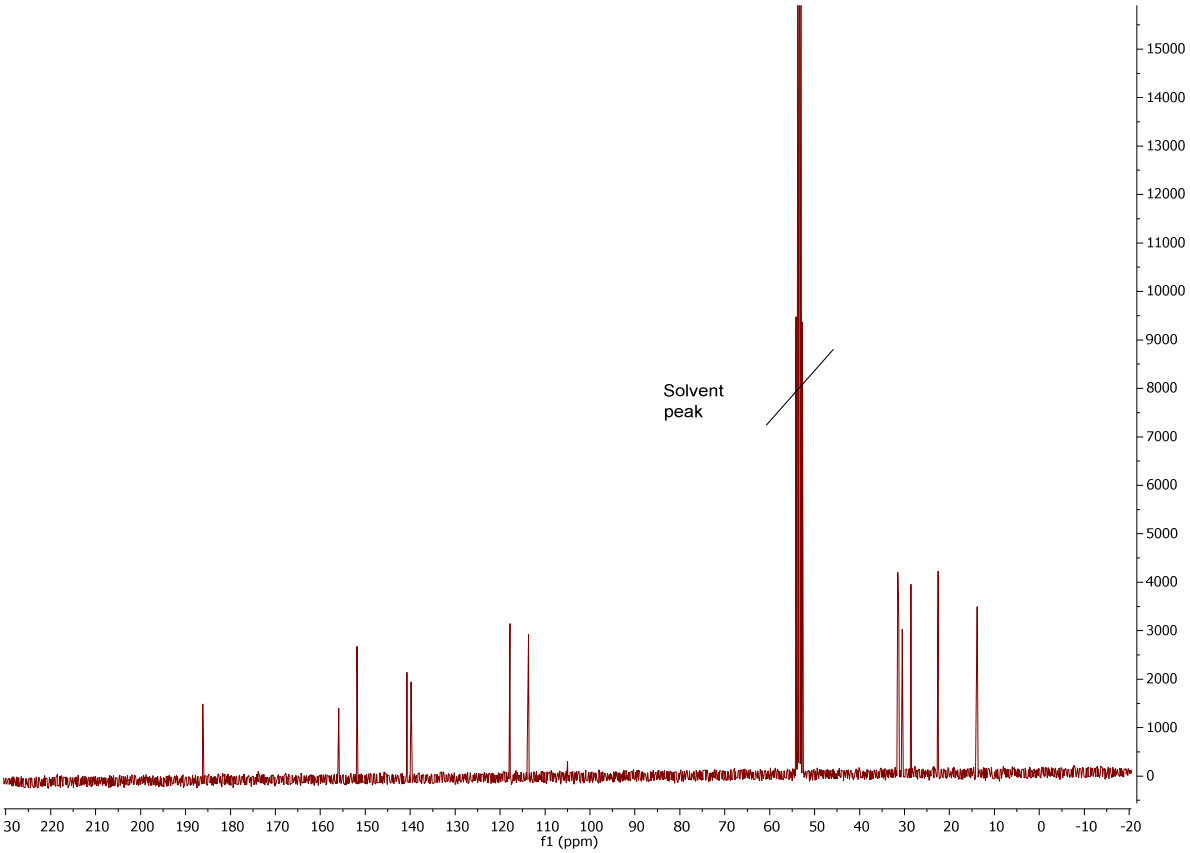

2,7-dihexyl-s-indaceno[1,2-b:5,6-b']bisthiophene-4,9-dione

DEPT in CD_2Cl_2

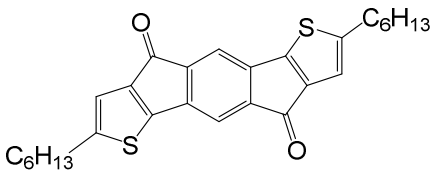

***Para*-IDT(=O)$_2$**

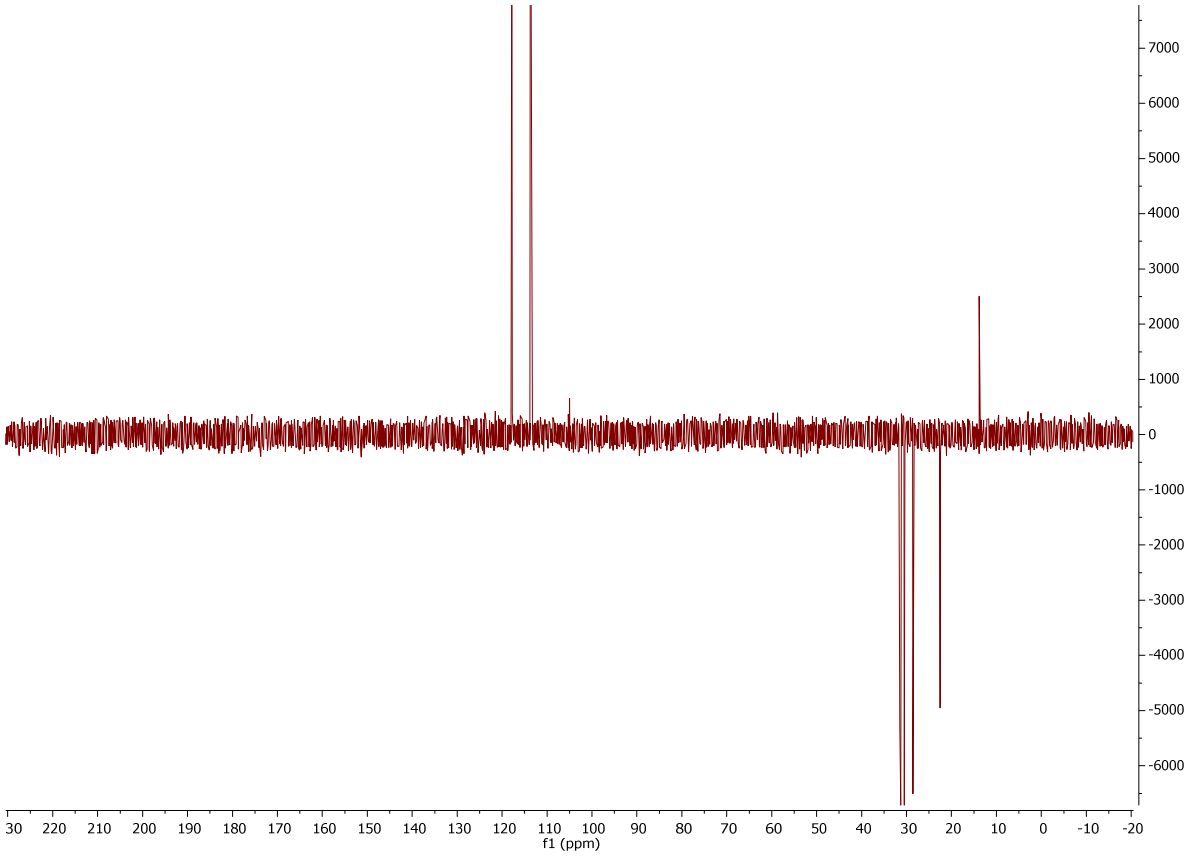

2,2'-(2,7-dihexyl-s-indaceno[1,2-b:5,6-b']bisthiophene-4,9-diylidene)dipropanedinitrile

^{1}H NMR in Tetrachloroethane

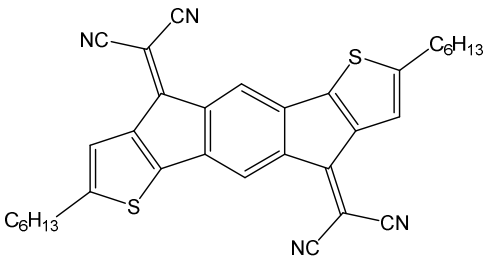

***Para*-IDT(=C(CN)$_2$)$_2$**

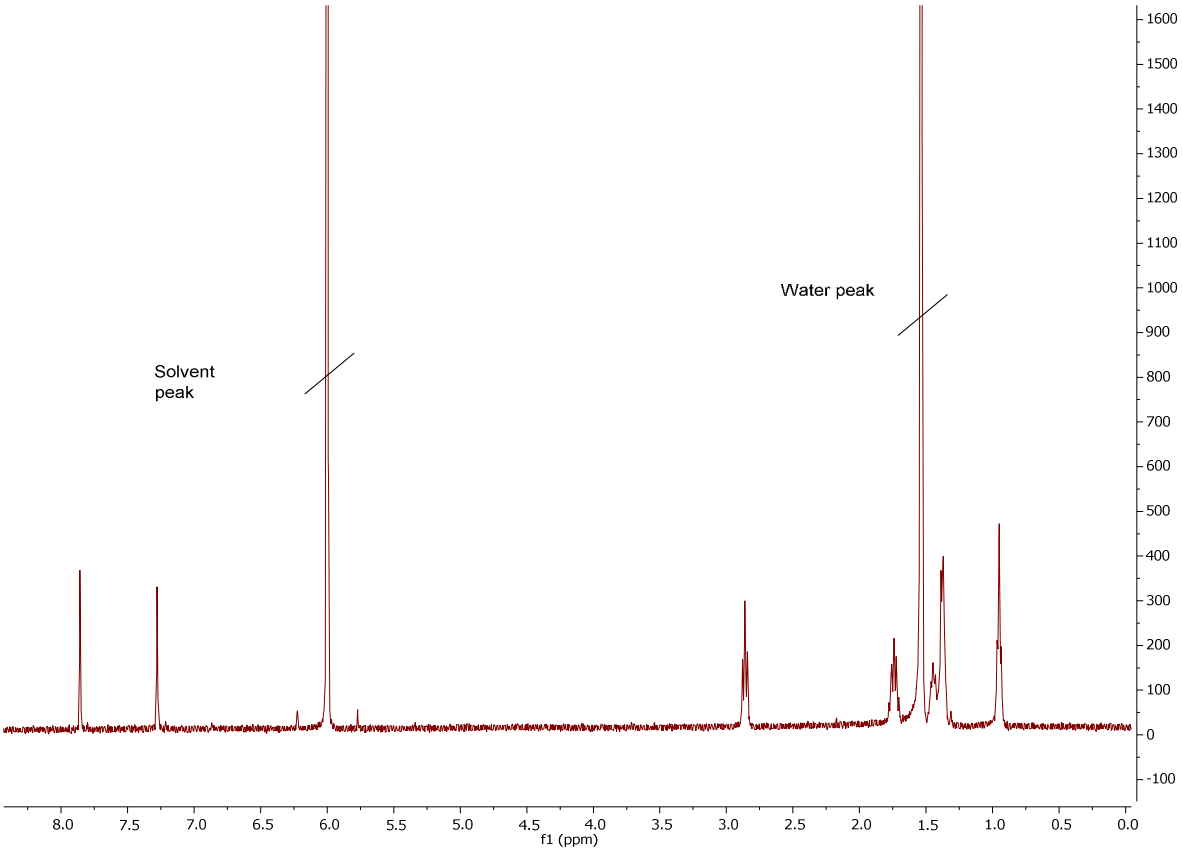

2,2'-(2,7-dihexyl-s-indaceno[1,2-b:5,6-b']bisthiophene--4,9-diylidene)dipropanedinitrile

^{13}C NMR in Tetrachloroethane

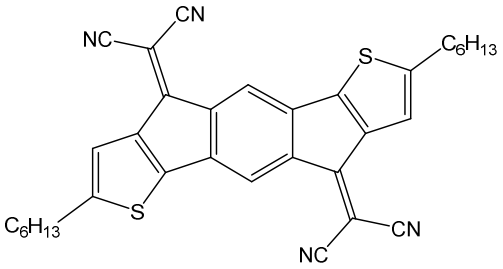

***Para*-IDT(=C(CN)$_2$)$_2$**

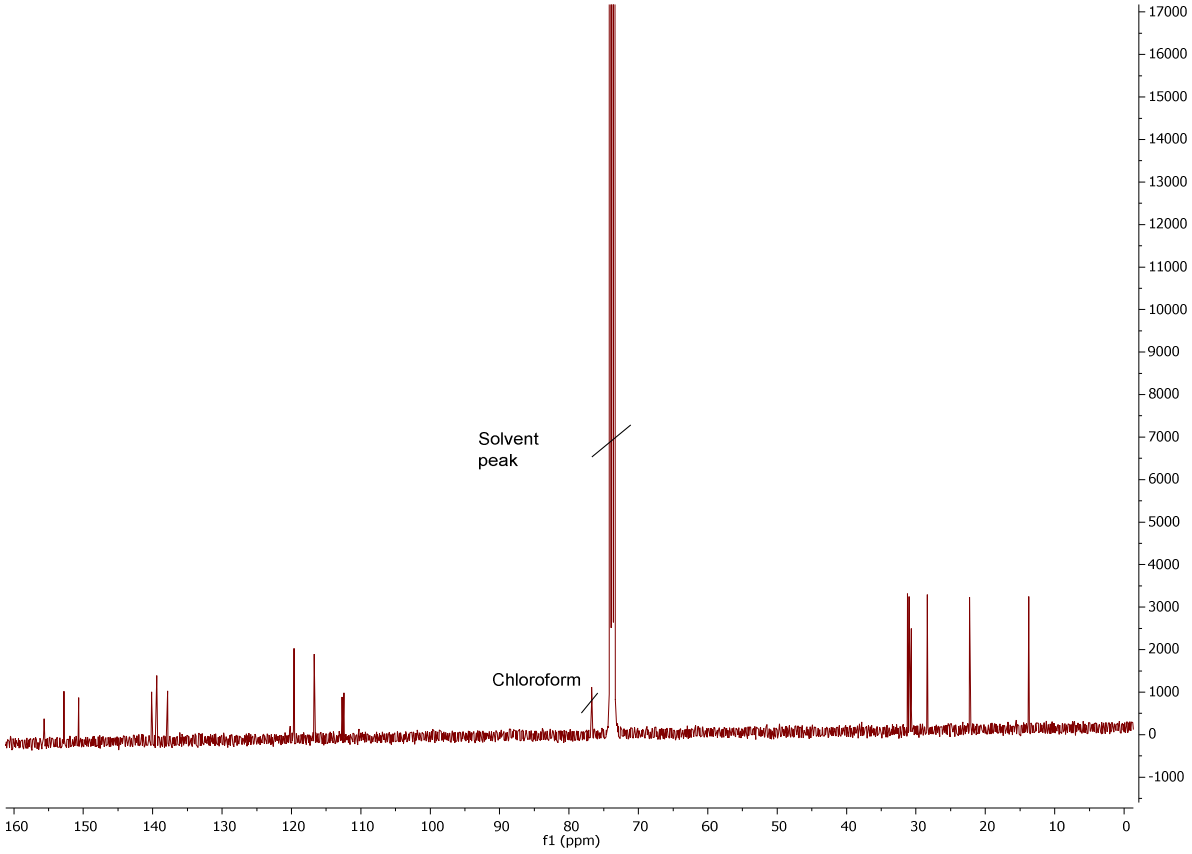

diethyl 4,6-bis(5-hexylthiophen-2-yl)isophthalate

^{1}H NMR in CD_2Cl_2

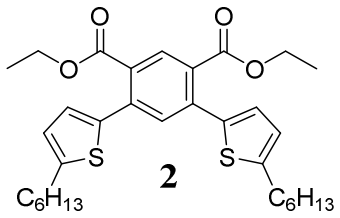

2

diethyl 4,6-bis(5-hexylthiophen-2-yl)isophthalate

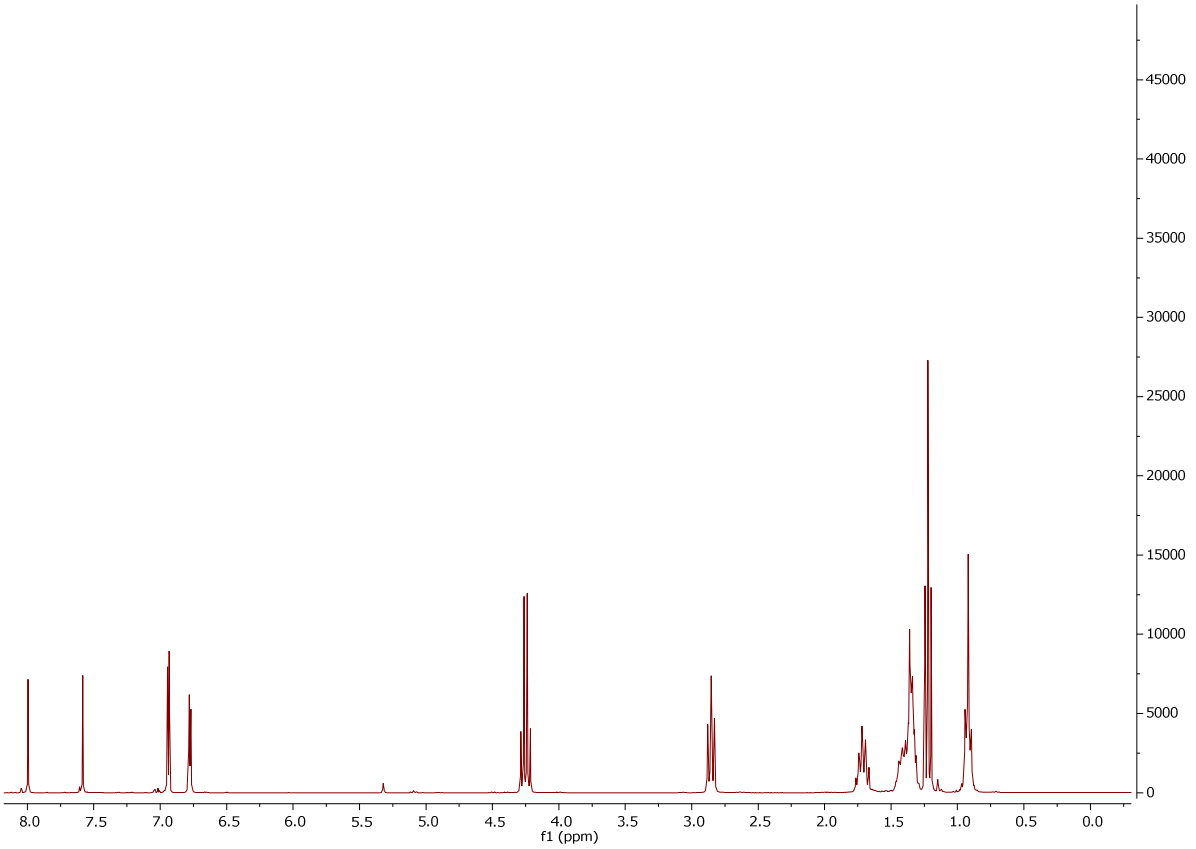

diethyl 4,6-bis(5-hexylthiophen-2-yl)isophthalate

^{13}C NMR in CD_2Cl_2

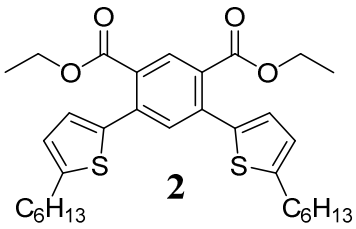

2

diethyl **4**,6-bis(5-hexylthiophen-2-yl)isophthalate

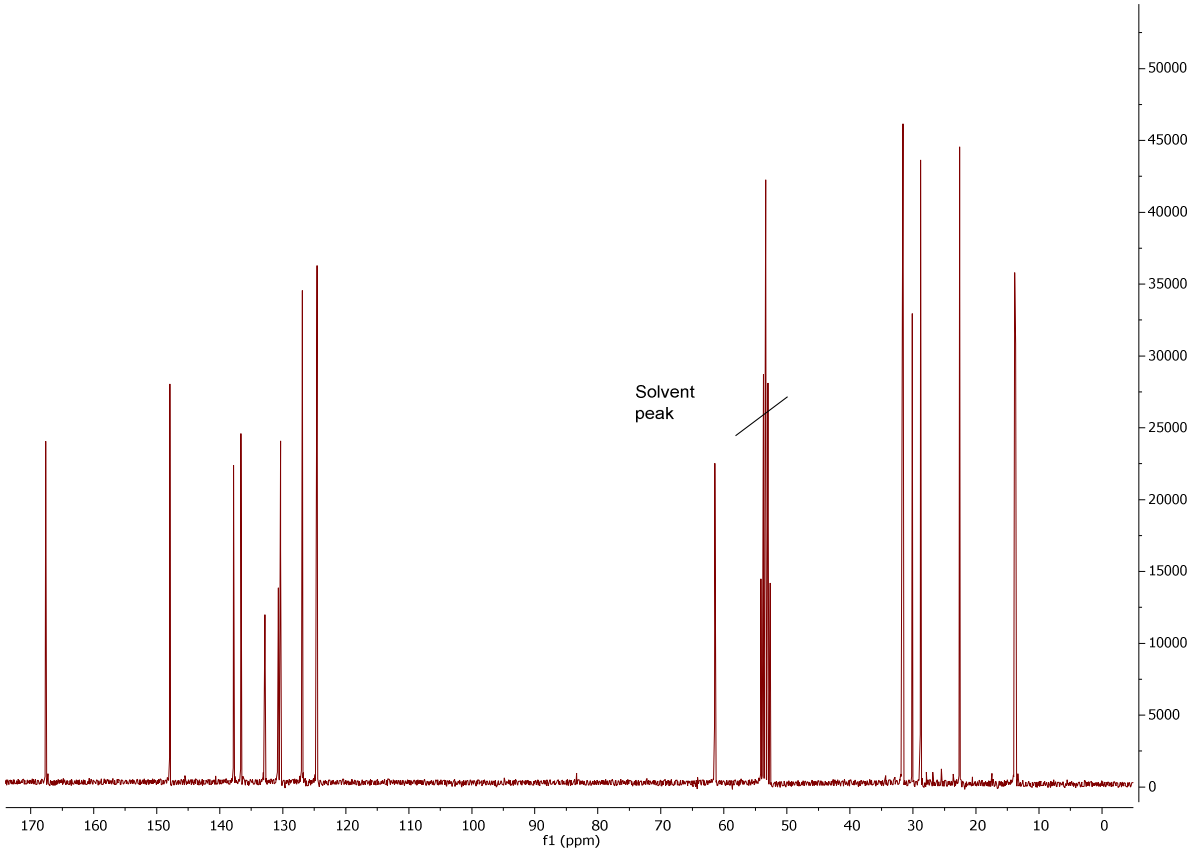

diethyl 4,6-bis(5-hexylthiophen-2-yl)isophthalate

DEPT in CD_2Cl_2

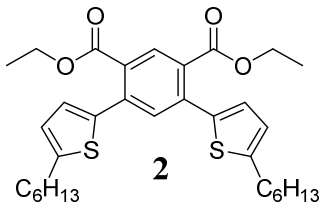

2

diethyl 4,6-bis(5-hexylthiophen-2-yl)isophthalate

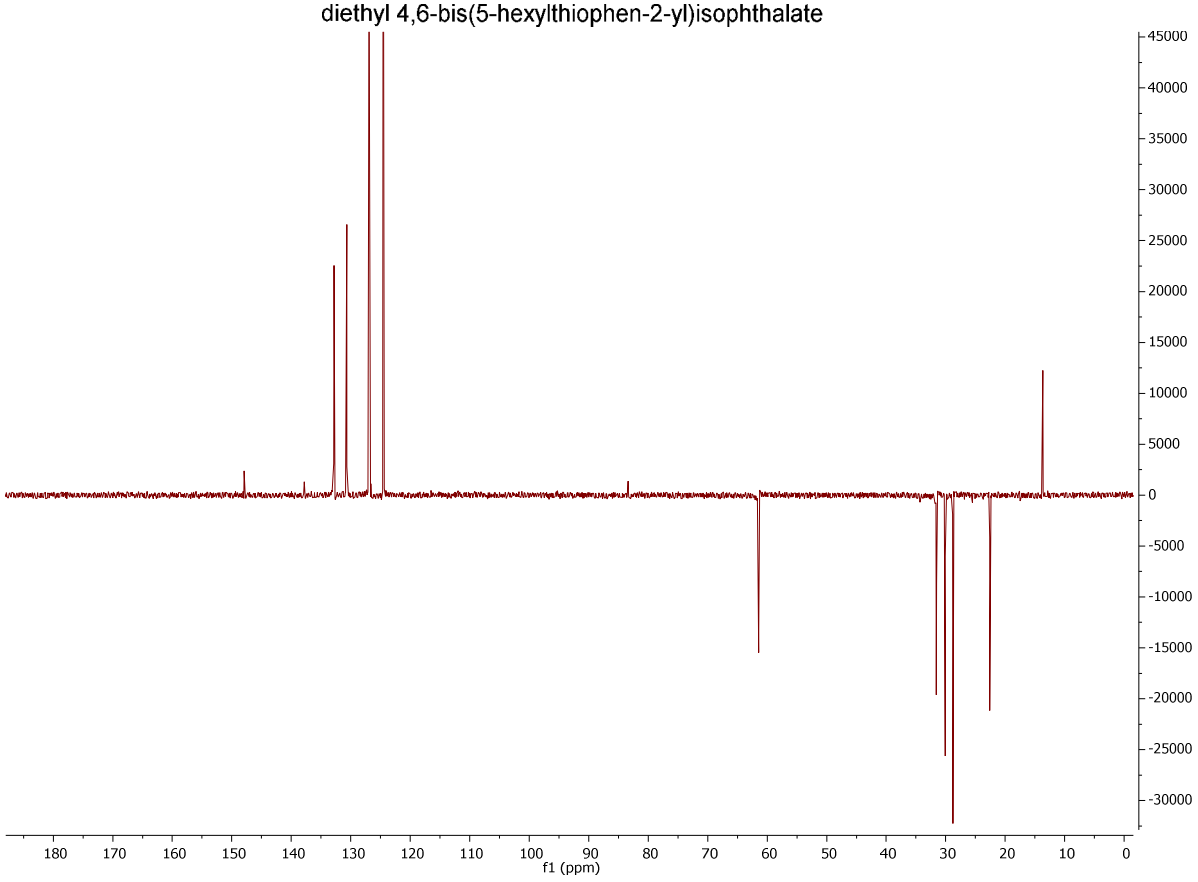

4,6-bis(5-hexylthiophen-2-yl)isophthalic acid

^{1}H NMR in DMSO

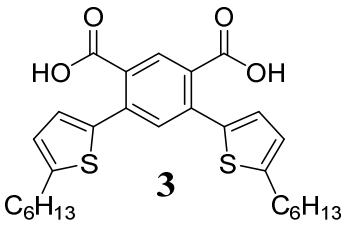

3

4,6-bis(5-hexylthiophen-2-yl)isophthalic acid

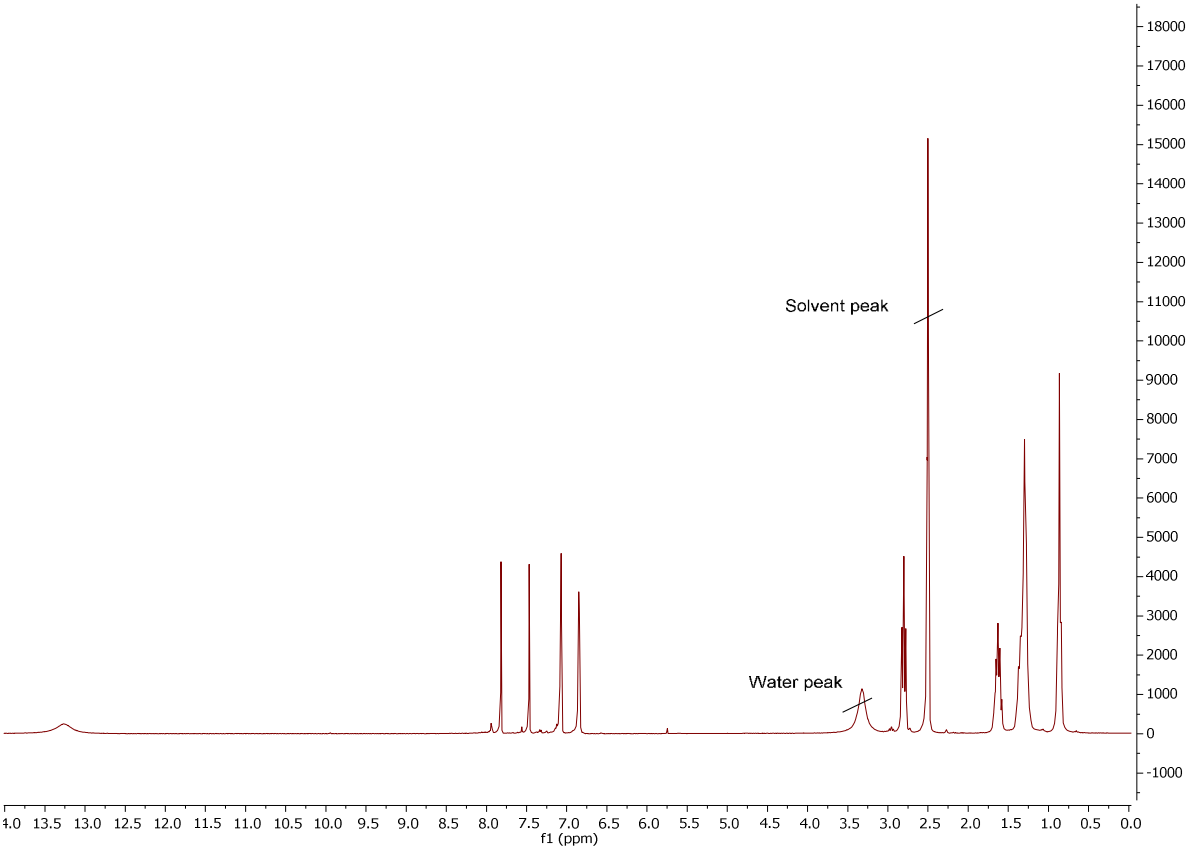

4,6-bis(5-hexylthiophen-2-yl)isophthalic acid

^{13}C NMR in DMSO

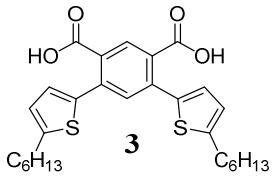

3

4,6-bis(5-hexylthiophen-2-yl)isophthalic acid

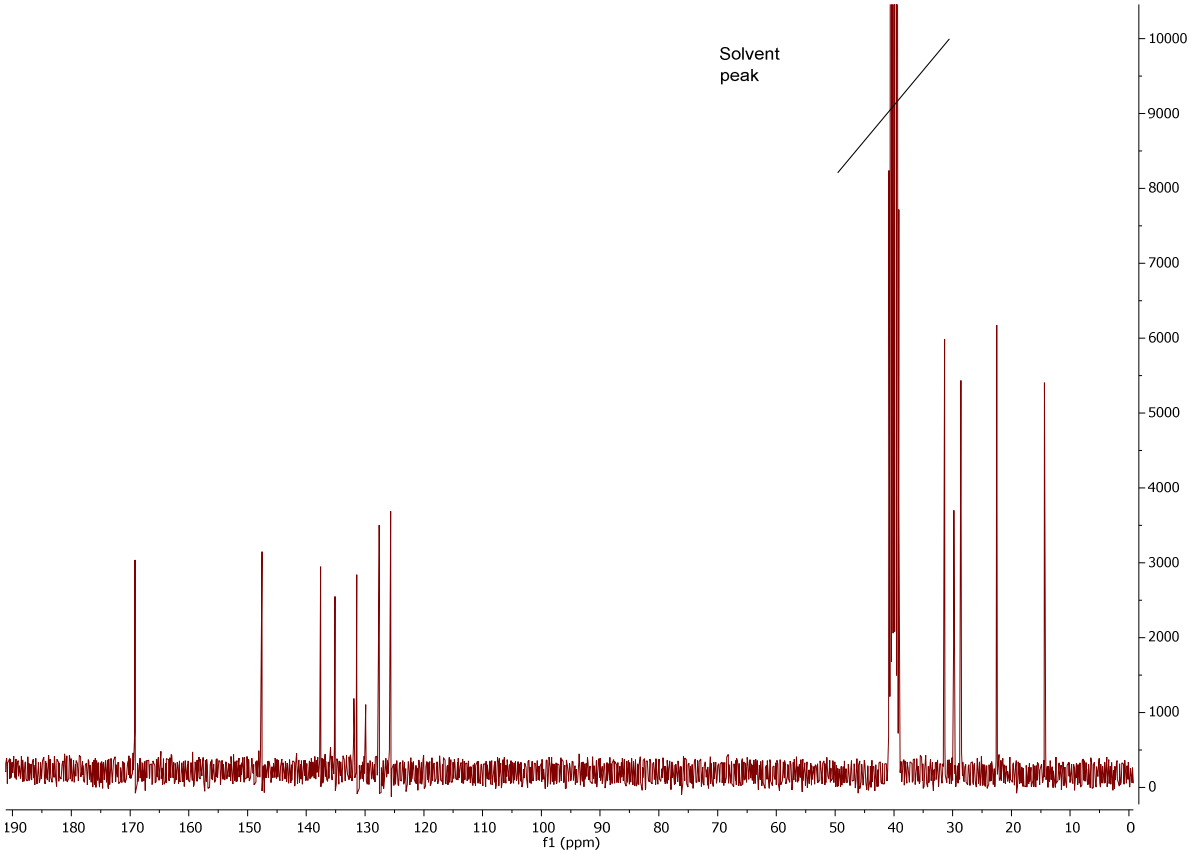

4,6-bis(5-hexylthiophen-2-yl)isophthalic acid

DEPT in DMSO

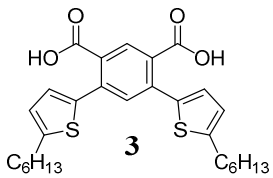

3

4,6-bis(5-hexylthiophen-2-yl)isophthalic acid

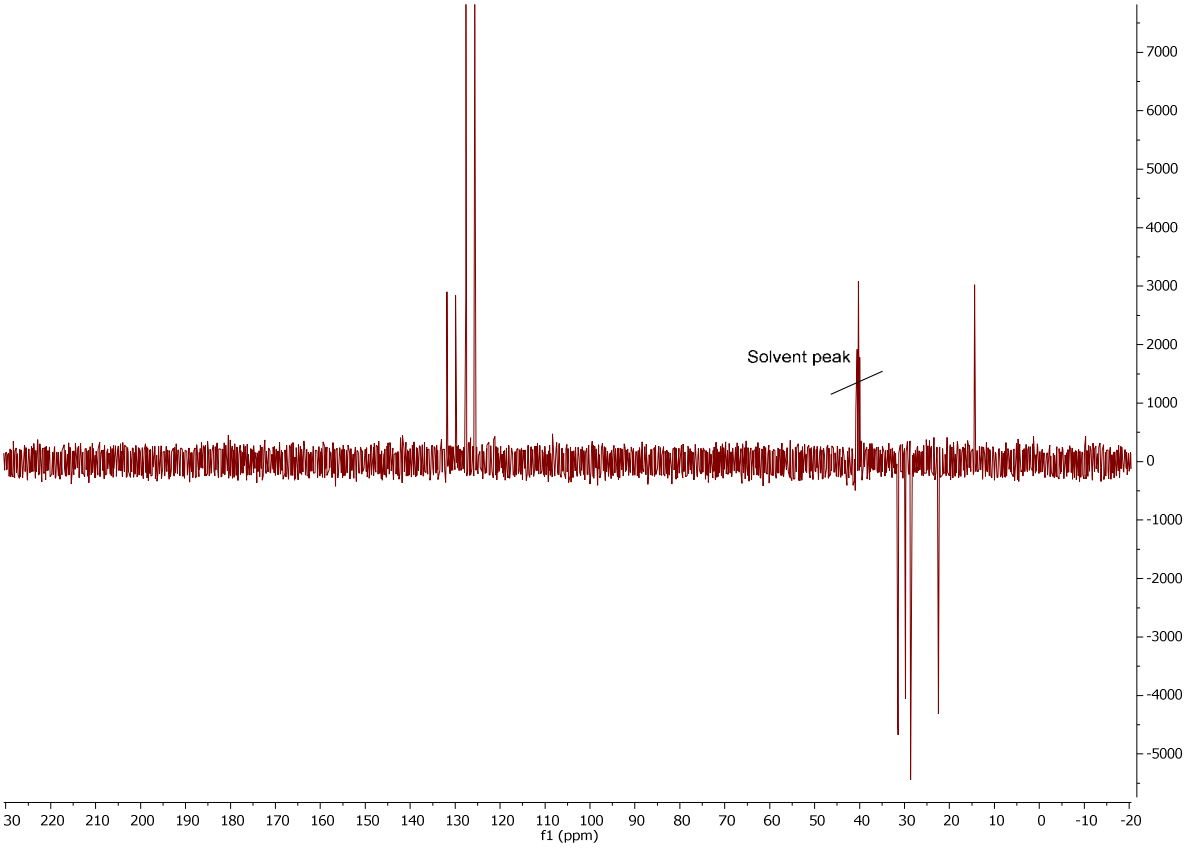

2,8-dihexyl-s-indaceno[1,2-b:7,6-b']dithiophene-4,6-dione

^{1}H NMR in CD_2Cl_2

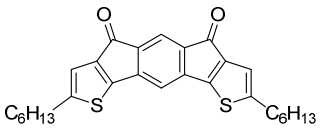

***meta*-IDT(=O)$_2$**

2,8-dihexyl-*s*-indaceno[1,2-*b*:7,6-*b*']dithiophene-4,6-dione

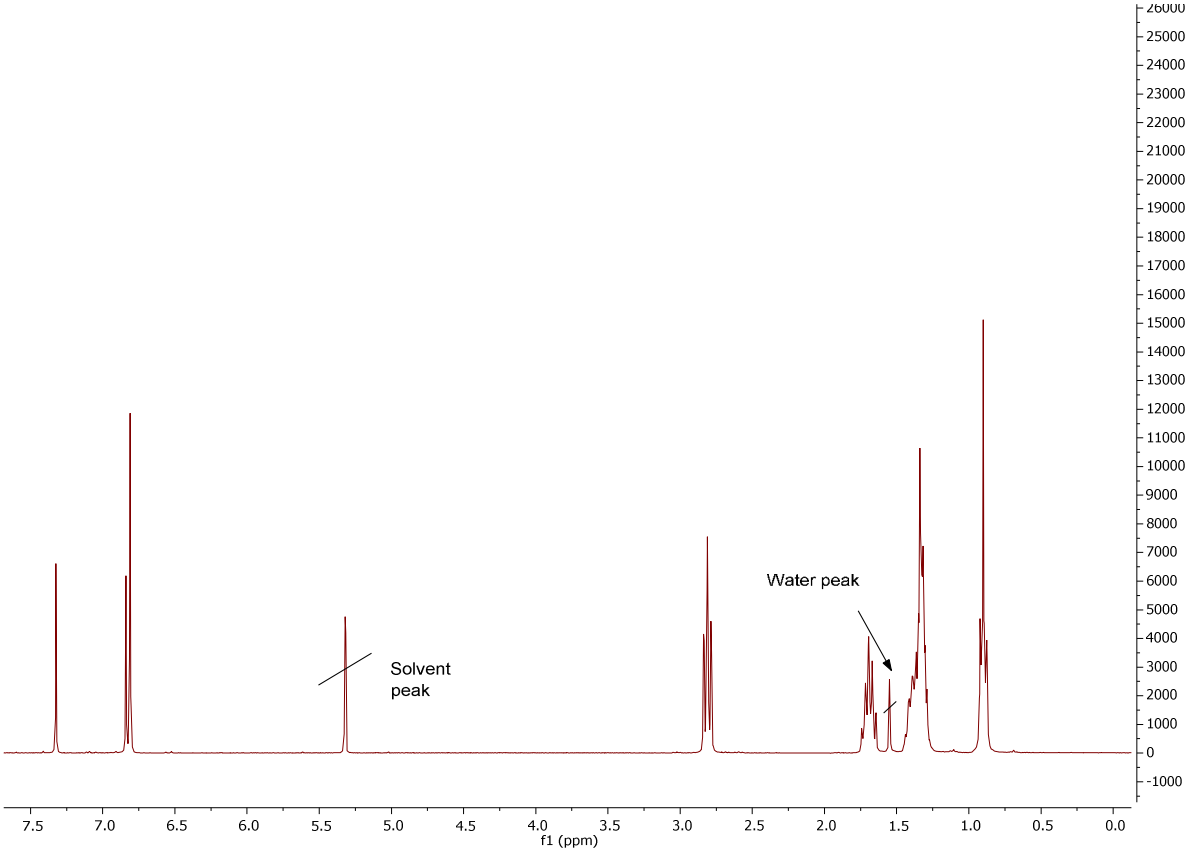

2,8-dihexyl-s-indaceno[1,2-b:7,6-b']dithiophene-4,6-dione

^{13}C NMR in CD_2Cl_2

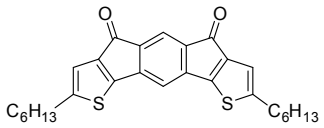

***meta*-IDT(=O)$_2$**

2,8-dihexyl-*s*-indaceno[1,2-*b*:7,6-*b*']dithiophene-4,6-dione

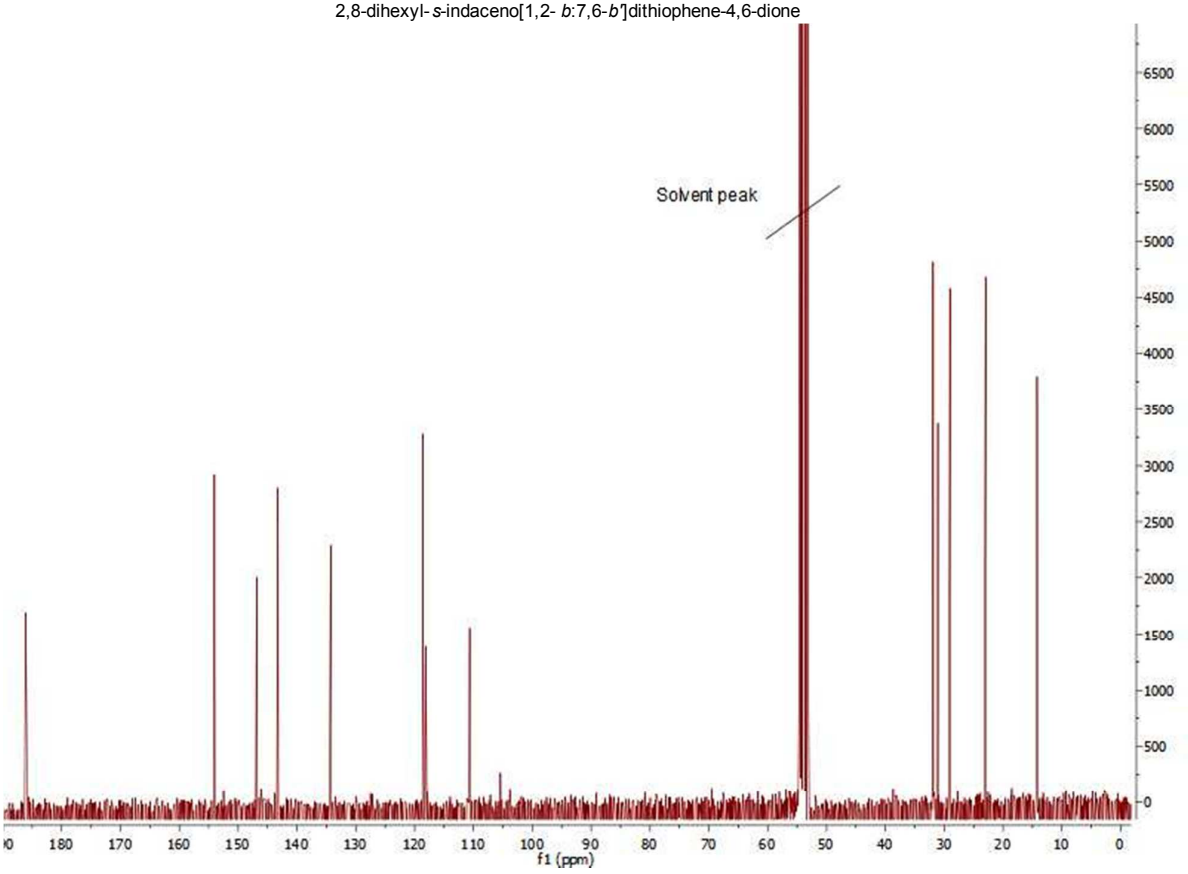

2,8-dihexyl-s-indaceno[1,2-b:7,6-b']dithiophene-4,6-dione

DEPT in CD_2Cl_2

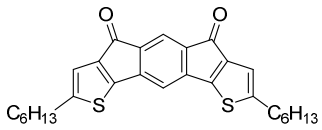

***meta*-IDT(=O)$_2$**

2,8-dihexyl-*s*-indaceno[1,2-*b*:7,6-*b*']dithiophene-4,6-dione

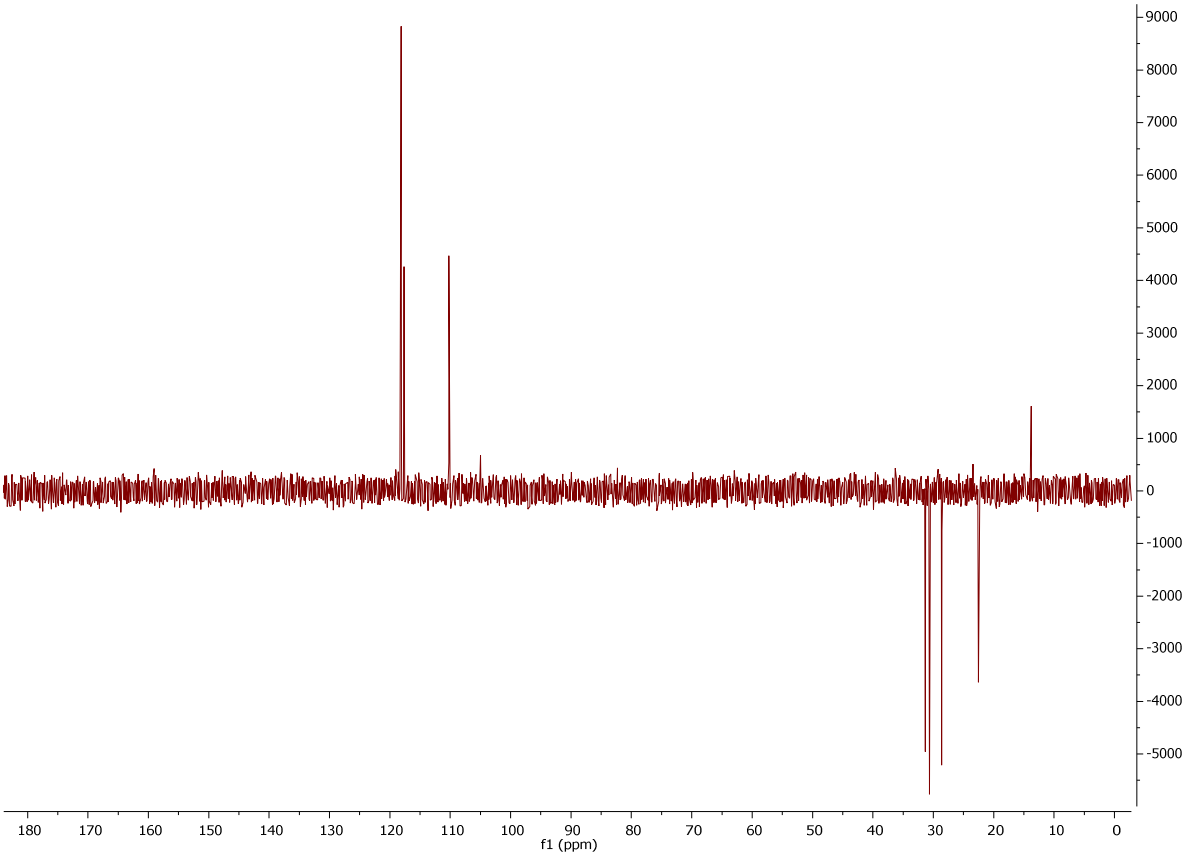

2,2'-(2,8-dihexyl-s-indaceno[1,2-b:7,6-b']dithiophene-4,6-diylidene)dimalononitrile

^{1}H NMR in Tetrachloroethane

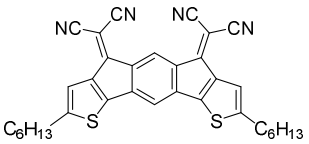

***meta*-IDT(=C(CN)$_2$)$_2$**

2,2'-(2,8-dihexyl-*s*-indaceno[1,2-*b*:7,6-*b*']dithiophene-4,6-diylidene)dimalononitrile

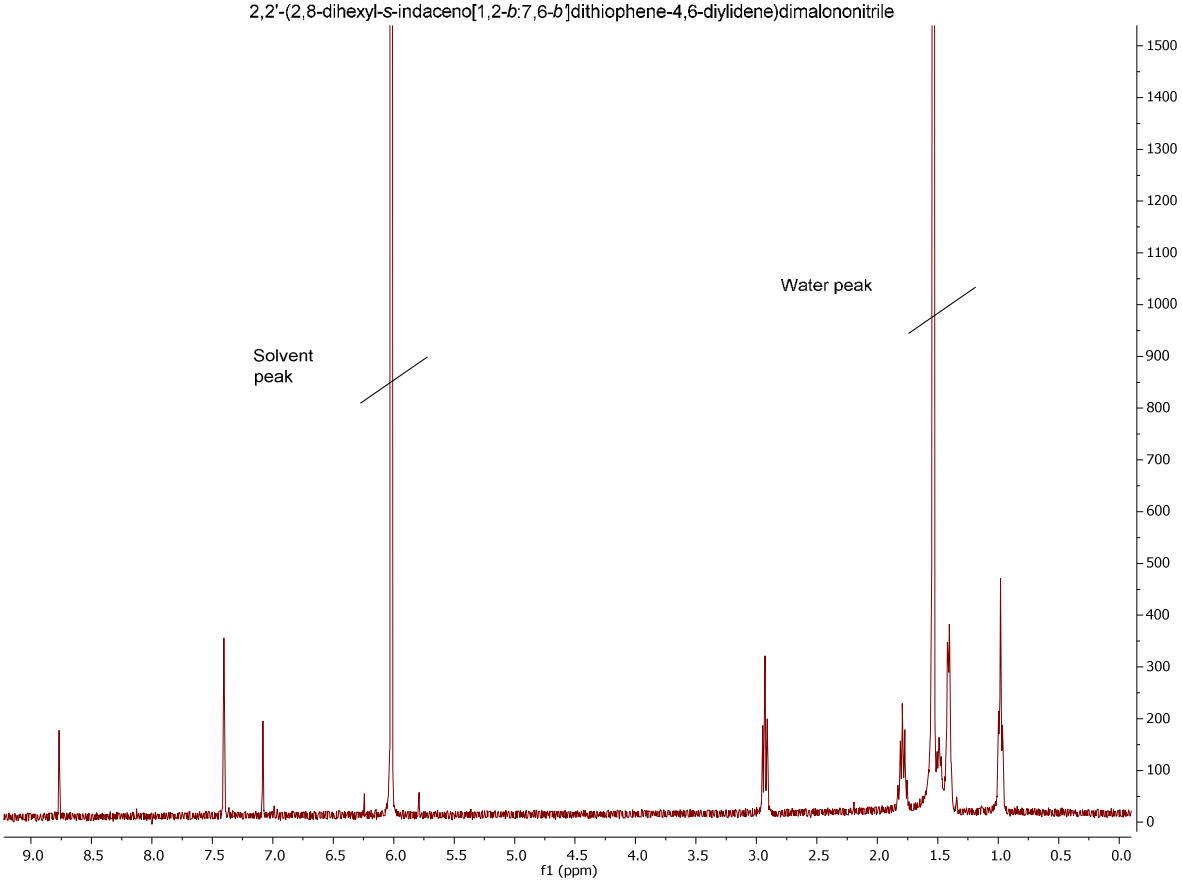

,2'-(2,8-dihexyl-s-indaceno[1,2-b:7,6-b']dithiophene-4,6-diylidene)dimalononitrile

^{13}C NMR in Tetrachloroethane

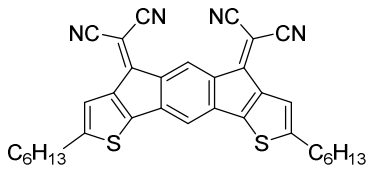

***meta*-IDT(=C(CN)$_2$)$_2$**

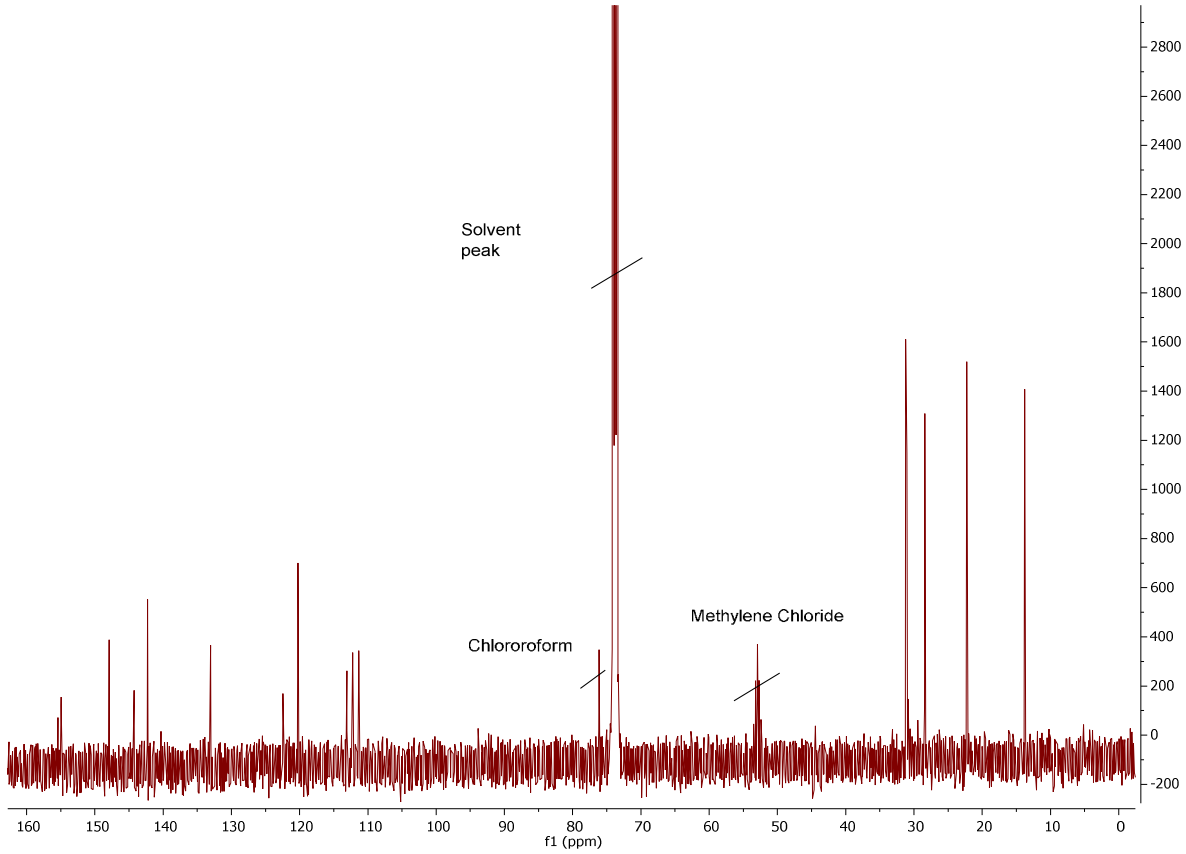

REFERENCES

1. Tian, H.; Deng, Y.; Pan, F.; Huang, L.; Yan, D.; Geng, Y.; Wang, F. A Feasibly Synthesized Ladder-Type Conjugated Molecule as the Novel High Mobility N-Type Organic Semiconductor *J. Mater. Chem.* **2010,** *20*, 7998-8004.
2. Kulkarni, A. P.; Tonzola, C. J.; Babel, A.; Jenekhe, S. A. Electron Transport Materials for Organic Light-Emitting Diodes. *Chem. Mater.* **2004,** *16*, 4556–4573.
3. Hohenberg, P.; Kohn, W. Inhomogeneous Electron Gas. *Phys. Rev.* **1964,** *136*, B864-B871.
4. Calais, J.-L. Book Review. *Int. J. Quantum Chem.* **1993,** *47*, 101.
5. Becke, A. D. Density-Functional Exchange-Energy Approximation with Correct Asymptotic Behavior. *Phys. Rev. A* **1988,** *38*, 3098-3100.
6. Becke, A. D. Density-Functional Thermochemistry. Iii. The Role of Exact Exchange. *J. Chem. Phys.* **1993,** *98*, 5648 –5652.
7. Becke, A. D. A New Mixing of Hartree–Fock and Local Density-Functional Theories. *J. Chem. Phys.* **1993,** *98*, 1372-1377.
8. Lee, C.; Yang, W.; Parr, R. G. Development of the Colle-Salvetti Correlation-Energy Formula into a Functional of the Electron Density. *Phys. Rev. B* **1988,** *37*, 785-789.
9. Frisch, M. J.; Trucks, G. W.; Schlegel, H. B.; Scuseria, G. E.; Robb, M. A.; Cheeseman, J. R.; Scalmani, G.; Barone, V.; Mennucci, B.; Petersson, G. A.; Nakatsuji, H.; Caricato, M.; Li, X.; Hratchian, H. P.; Izmaylov, A. F.; Bloino, J.; Zheng, G.; Sonnenberg, J. L.; Hada, M.; Ehara, M.; Toyota, K.; Fukuda, R.; Hasegawa, J.; Ishida, M.; Nakajima, T.; Honda, Y.; Kitao, O.; Nakai, H.; Vreven, T.; Montgomery, J. A. J.; Peralta, J. E.; Ogliaro, F.; Bearpark, M.; Heyd, J. J.; Brothers, E.; Kudin, K. N.; Staroverov, V. N.; Keith, T.; Kobayashi, R.; Normand, J.; Raghavachari, K.; Rendell, A.; Burant, J. C.; Iyengar, S. S.; Tomasi, J.; Cossi, M.; Rega, N.; Millam, J. M.; Klene, M.; Knox, J. E.; Cross, J. B.; Bakken, V.; Adamo, C.; Jaramillo, J.; Gomperts, R.; Stratmann, R. E.; Yazyev, O.; Austin, A. J.; Cammi, R.; Pomelli, C.; Ochterski, J. W.; Martin, R. L.; Morokuma, K.; Zakrzewski, V. G.; Voth, G. A.; Salvador, P.; Dannenberg, J. J.; Dapprich, S.; Daniels, A. D.; Farkas, O.; Foresman, J. B.; Ortiz, J. V.; Cioslowski, J.; Fox, D. J. *Gaussian 09*, Revision B.01; Gaussian, Inc.: Wallingford, Ct, 2010.
10. MicroChem Su-8 2000 Permanent Epoxy Negative Photoresist Processing Guidelines for Su-8 2000.5, Su-8 2002, So-8 2005, Su-8 2007, Su-8 2010 and Su-8 2015. http://www.micro-chem.com/pdf/SU-82000DataSheet2000_5thru2015Ver4.pdf (accessed 13/09/2006).
11. Richards, T.; Sirringhaus, H. Bias-Stress Induced Contact and Channel Degradation in Staggered and Coplanar Organic Field-Effect Transistors *Appl. Phys. Lett.* **2008,** *92*, 023512-1/12.
12. Kim, C. H.; Bonnassieux, Y.; Horowitz, G. Fundamental Benefits of the Staggered Geometry for Organic Field-Effect Transistors. *IEEE Electr. Device L.* **2011,** *32*, 1302 - 1304.
13. Pesavento, P. V.; Chesterfield, R. J.; Newman, C. R.; Frisbie, C. D. Gated Four-Probe Measurements on Pentacene Thin-Film Transistors: Contact Resistance as a Function of Gate Voltage and Temperature. *J. Appl. Phys.* **2004,** *96*, 7312.